



HAL
open science

Identification of sources of potential fields with the continuous wavelet transform: Complex wavelets and application to aeromagnetic profiles in French Guiana

Pascal Sailhac, Armand Galdeano, Dominique Gibert, Frédérique Moreau,
Claude Delor

► To cite this version:

Pascal Sailhac, Armand Galdeano, Dominique Gibert, Frédérique Moreau, Claude Delor. Identification of sources of potential fields with the continuous wavelet transform: Complex wavelets and application to aeromagnetic profiles in French Guiana. *Journal of Geophysical Research: Solid Earth*, 2000, 105, pp.19,455-19,475. 10.1029/2000JB900090 . insu-03596933

HAL Id: insu-03596933

<https://insu.hal.science/insu-03596933>

Submitted on 4 Mar 2022

HAL is a multi-disciplinary open access archive for the deposit and dissemination of scientific research documents, whether they are published or not. The documents may come from teaching and research institutions in France or abroad, or from public or private research centers.

L'archive ouverte pluridisciplinaire **HAL**, est destinée au dépôt et à la diffusion de documents scientifiques de niveau recherche, publiés ou non, émanant des établissements d'enseignement et de recherche français ou étrangers, des laboratoires publics ou privés.

Copyright

Identification of sources of potential fields with the continuous wavelet transform: Complex wavelets and application to aeromagnetic profiles in French Guiana

Pascal Sailhac and Armand Galdeano

Laboratoire de Géomagnétisme, Institut de Physique du Globe de Paris, Paris, France.

Dominique Gibert and Frédérique Moreau

Géosciences Rennes, Université de Rennes 1, Rennes, France.

Claude Delor

Bureau des Recherches Géologiques et Minières, Orléans, France.

Abstract. A continuous wavelet technique has been recently introduced to analyze potential fields data. First, we summarize the theory, which primarily consists of interpreting potential fields via the properties of the upward continued derivative field. Using complex wavelets to analyze magnetic data gives an inverse scheme to find the depth and homogeneity degree of local homogeneous sources and the inclination of their magnetization vector. This is analytically applied on several local and extended synthetic magnetic sources. The application to other potential fields is also discussed. Then, profiles crossing dikes and faults are extracted from the recent high-resolution aeromagnetic survey of French Guiana and analyzed using complex one dimensional wavelets. Maps of estimated depth to sources and their magnetization inclination and homogeneity degree are proposed for a region between Cayenne and Kourou.

1. Introduction

The high resolution of recent magnetic (and gravity) surveys [Gunn, 1997; Biegert and Millegan, 1998; Grauch and Millegan, 1998] stimulates the development of specific interpretation techniques which emphasize the information of interest to the geologist and to the geophysicist: Modern magnetometers measure the magnetic field to ~ 0.01 nT (the Earth's dipole magnetic field is $\sim 30,000$ - $60,000$ nT worldwide, with an amplitude of the anomaly due to the upper crust of hundreds of nanoteslas); Global Positioning Systems (GPS) can give the position from a few meters (in aeromagnetic surveys) to a few centimeters (in ground surveys).

We have explored the use of wavelet transforms, as initially introduced in the analysis of potential fields by Moreau [1995]. She has described the technique for local and extended sources, with the emphasis on gravity applications, followed by preliminary results for magnetic cases. The principle of this method is to interpret potential fields data via the properties of the upward continued derivative field. Moreau *et al.* [1997]

have demonstrated the general n -dimensional theory for local homogeneous sources. Moreau *et al.* [1999] have analyzed the effects of noise and extent of sources on the properties of the wavelet coefficients. We now present specific properties of the one-dimensional (1-D) complex wavelet coefficients of the total field magnetic anomaly: Apparent inclination of magnetization, in addition to depth, vertical extent, and dip angle of sources can be estimated. This wavelet technique applied to magnetic studies is not only a filtering as used in recent advances in aeromagnetic processing [Fedi and Quarta, 1998; Ridsdull-Smith and Dentith, 1999] but actually gives the derivatives (and analytic signal) of the upward continued anomaly field. This is more like the continuous wavelet analysis developed for the location of singular features of the source distribution [Hornby *et al.*, 1999], which is improved when scaling relations of the wavelet coefficients are analyzed and when vertical derivatives are used in addition to the horizontal derivatives. This complementary development to existing upward continuation techniques [Paul *et al.*, 1966] and to recent advances in the interpretation of the gradients of potential fields [Pedersen and Rasmussen, 1990; Pilkington, 1997; Hsu *et al.*, 1998], provides a theoretical framework to enlighten properties of the sources via their scaling character.

Copyright 2000 by the American Geophysical Union.

Paper number 2000JB900090.
0148-0227/00/2000JB900090\$09.00

First, we have applied this technique to several local and extended synthetic magnetic sources: Local elementary magnetization (dipole), local multipole magnetization, vertical and inclined steps, strips, and prisms of magnetization. Wavelet coefficients have been calculated for the total magnetic anomaly field at any normal apparent inclination.

Then, we have applied the technique to data profiles from French Guiana. A set of 27 profiles each of 80 km long with flightline direction N30°E has been transformed by wavelets; for the purpose of this study we have analyzed three isolated features in the Cayenne-Kourou area: two dikes and one fault.

2. Method

2.1. Wavelet Transform of Potential Fields

First, we briefly recall the basic theory [Moreau et al., 1997, 1999], which we apply to the case of a two-dimensional physical space. This involves parameters that are listed in the notation section. We define the continuous wavelet transform of a function $\phi_0(x \in \mathbb{R})$ as a convolution product,

$$\begin{aligned} \mathcal{W}_{\psi|\phi_0}(b, a) &= \int_{\mathbb{R}} \frac{dx}{a} \psi\left(\frac{b-x}{a}\right) \phi_0(x) \\ &= (\mathcal{D}_a \psi * \phi_0)(b), \end{aligned} \tag{1}$$

where $\psi(x \in \mathbb{R})$ is the analyzing wavelet, $a \in \mathbb{R}^+$ is a dilation parameter, and the dilation operator \mathcal{D}_a is defined by

$$\mathcal{D}_a \psi(x) = \frac{1}{a} \psi\left(\frac{x}{a}\right). \tag{2}$$

The source is modeled as a homogeneous function $\sigma(x, z)$. This means, for instance, when the source is homogeneous at $x = 0$ and $z = 0$ with homogeneity degree α , that for any positive number λ it follows that $\sigma(\lambda x, \lambda z) = \lambda^\alpha \sigma(x, z)$.

By applying a Fourier multiplier homogeneous of degree γ (equivalent to a derivative of order γ) and a dilation to the Poisson semigroup kernel [Moreau et al.,

1997, 1999], we obtain a class of wavelets ψ^γ (Figure 1) for which the wavelet coefficients of a potential field due to local homogeneous sources exhibit simple properties. For the potential field $\phi(x, z = 0)$ measured at level $z = 0$ which is due to a local homogeneous source located at $x = 0$ and depth $z = z_0$, the wavelet coefficients in the upper half plane of positions and dilations ($a = -z > 0$) obey a double scaling law with two exponent parameters:

$$\begin{aligned} \mathcal{W}_{\psi^\gamma|\phi(\cdot, z=0)}(x, a) &= \\ \left(\frac{a}{a'}\right)^\gamma \left(\frac{a' + z_0}{a + z_0}\right)^{-\beta} &\mathcal{W}_{\psi^\gamma|\phi(\cdot, z=0)}\left(x \frac{a' + z_0}{a + z_0}, a'\right). \end{aligned} \tag{3}$$

In (3), x and a are the position and the dilation, respectively, for the left-hand side wavelet coefficient; $x(a' + z_0)/(a + z_0)$ and a' are the position and the dilation, respectively, for the right-hand side wavelet coefficient: This defines a set of lines (x, a) which satisfy $x/(z_0 + a) = \text{const}$. For various constants we obtain a family of lines that intersect at the point $(0, -z_0)$ inside the lower half plane; therefore the wavelet transform exhibits a cone-like structure where the top of the cone is shifted to the location of the source: Using the modulus maxima lines (on which the signal to noise ratio is the best), this constitutes a geometrical procedure to obtain the location of a homogeneous local source with no a priori idea of its homogeneity degree (see Figure 2). The first exponent γ is the order of the wavelet ψ^γ which has been used, the second exponent β is associated with the homogeneity degree of the source α ($\beta = \alpha - \gamma$ for the total geomagnetic field anomaly). Once the depth z_0 of the anomaly field has been obtained, the exponent β is simply obtained with the wavelet coefficients \mathcal{W}_a along modulus maxima lines as the slope of $\log(|\mathcal{W}_a|/a^\gamma)$ versus $\log(a + z_0)$ (Figure 2).

The kernel of the Poisson semigroup which is used to build these special wavelets defines the well-known upward continuation filter $P_a(x)$ which transforms the harmonic field $\phi(\cdot, z)$ from measured level z to the level $z + a$ [Le Mouél, 1970; Bhattacharyya, 1972; Galdeano,

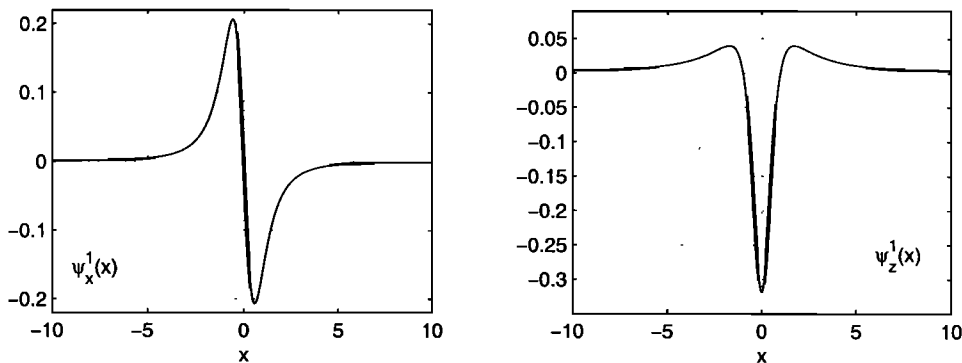


Figure 1. Typical wavelets belonging to the Poisson semigroup class: $\Psi_x^1(x) = (1/\pi)[-2x/(x^2 + 1)^2]$ and $\Psi_z^1(x) = (1/\pi)[(x^2 - 1)/(x^2 + 1)^2]$.

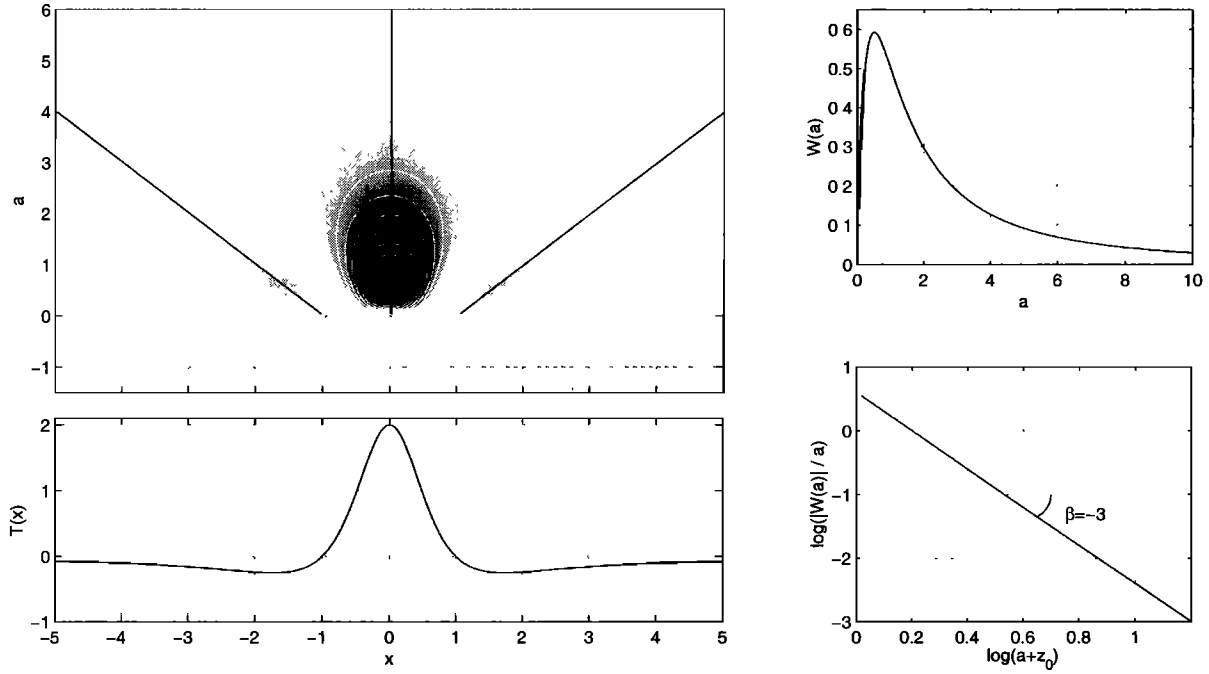


Figure 2. (bottom left) Magnetic total field T due to a vertical dipole at $x_0 = 0$ and $z_0 = 1$ analyzed with vertical wavelet ψ_z^1 : (top left) Modulus maxima lines converge at the location of the source, at $x = x_0$ and $a = -z_0$ (with downward continuation in dotted lines); (right) the modulus along the line at $x = x_0$ follows a scaling relation with exponent $\beta = -3$ associated with the homogeneity degree of the local line source $\alpha = -2$.

1974; Baranov, 1975; Gibert and Galdeano, 1985]; x being a 1-D variable (abscissa along the profile), this is

$$P_a(x) = \frac{1}{\pi} \frac{a}{a^2 + x^2}. \tag{4}$$

Two typical real wavelets can then be considered, the “horizontal“ ψ_x , and the “vertical“ ψ_z made by one horizontal or one vertical (upward) derivative of P_1 respectively; they are said to be of order 1. Following with $\gamma - 1$ derivatives over x gives wavelets of order γ : $\psi_x^\gamma(x) = \partial_x^\gamma P_1(x)$ (or in Fourier domain: $\hat{\psi}_x^\gamma(u) = (i2\pi u)^\gamma e^{-2\pi|u|}$); $\psi_z^\gamma(x) = \partial_x^{\gamma-1} \partial_a P_a(x)|_{a=1}$ (or in Fourier domain: $\hat{\psi}_z^\gamma(u) = (i2\pi u)^{\gamma-1} (-2\pi|u|) e^{-2\pi|u|}$). Then dilating these wavelets with the dilation a transforms $\psi^\gamma(x)$ into $\psi^\gamma(x/a)/a$, which is also the γ th derivative of $P_a(x)$ multiplied by the scaling factor a^γ . Thus the convolution of the harmonic field $\phi(\cdot, z)$ (measured at level z) with these dilated real wavelets gives the wavelet coefficients at scale a which are also the derivatives of the upward continued field (at level $z+a$) whose dimension is that of the initial field (in nT for the geomagnetic total field anomaly):

$$\begin{aligned} \mathcal{W}_{\psi_x^\gamma|\phi(\cdot, z)}(x, a) &= a^\gamma \frac{\partial^{\gamma-1} \phi_x(x, z+a)}{\partial x^{\gamma-1}}, \\ \mathcal{W}_{\psi_z^\gamma|\phi(\cdot, z)}(x, a) &= a^\gamma \frac{\partial^{\gamma-1} \phi_z(x, z+a)}{\partial x^{\gamma-1}}, \end{aligned} \tag{5}$$

where $\phi_x(\cdot, z)$ and $\phi_z(\cdot, z)$ are the horizontal and up-

ward vertical derivatives, respectively, of the harmonic potential field $\phi(\cdot, z)$ at level z .

2.2. Complex Wavelets

Any of the two real wavelets ψ_x^γ and ψ_z^γ can be used to determine the depth and the homogeneity degree α of a local dipole source (Figure 2), but the determination of the inclination of this dipole needs the introduction of complex wavelets ψ_c^γ in order for this to be done in a simple way. Using the Hilbert transform \mathcal{H} , which changes ψ_x^γ into $\psi_z^\gamma = -\mathcal{H}[\psi_x^\gamma]$, we define the complex wavelets $\psi_c^\gamma = \psi_x^\gamma + i\mathcal{H}[\psi_x^\gamma]$ as combinations of the horizontal and vertical wavelets ψ_x^γ and ψ_z^γ [Moreau, 1995]: $\psi_c^\gamma = \psi_x^\gamma - i\psi_z^\gamma$. These are actually defined not only for $\gamma \in \mathbb{N}^*$ but for $\gamma \in \mathbb{R}_+^*$ (with the help of fractional derivatives). They are progressive wavelets proportional to the Cauchy wavelets [Holschneider, 1995], and their general expression is

$$\psi_c^\gamma(x) = \frac{e^{z\pi(\gamma+1)}}{\pi} \frac{i\Gamma(\gamma+1)}{(x+i)^{\gamma+1}}, \tag{6}$$

where Γ is the Gamma function. Thus the complex wavelet coefficients of the potential field $\phi(\cdot, z)$ are

$$\mathcal{W}_{\psi_c^\gamma|\phi(\cdot, z)}(x, a) = \mathcal{W}_{\psi_x^\gamma|\phi(\cdot, z)}(x, a) - i\mathcal{W}_{\psi_z^\gamma|\phi(\cdot, z)}(x, a). \tag{7}$$

where Γ is the Gamma function.

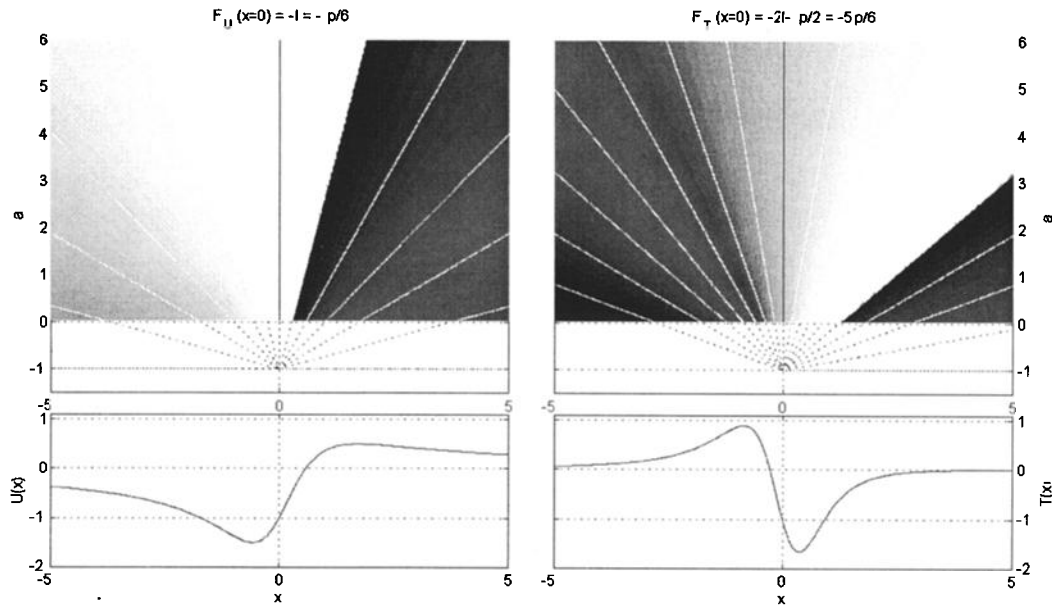


Figure 3. Magnetic potential U and total field T due to a dipole with inclination $I = \pi/6$ at $x_0 = 0$ and $z_0 = 1$ analyzed with complex wavelet ψ_c^1 : Phase isovalues (shown in white, every $\pi/6$) converge to the source (dotted lines); the phase isovalue $\Phi(x = 0)$ (for $x = x_0 = 0$) gives the inclination I .

For a local dipole of normal inclination I analyzed with a complex wavelet of order 1, the argument of the wavelet coefficients is constant along the vertical to the source, equal to $-I$ for the magnetic potential and to $-2I - \pi/2$ for the magnetic total field anomaly (Figure 3). Equation (3) shows that the isovalues of the phase of the complex wavelet coefficients also draw a cone-like structure pointing to the source (Figure 3).

2.3. Comparison With Classical Techniques

The complex wavelet coefficients $\mathcal{W}_{\psi_c^{\gamma+1}|\phi(\cdot,z)}(x,a)$ are associated with the upward continued analytic signal as early introduced to the interpretation of geophysical potential fields [Nabighian, 1972, 1974]:

$$\left(\left| \mathcal{W}_{\psi_c^{\gamma+1}|\phi(\cdot,z)}(x,a) \right| / a^{\gamma+1} \right)^2 = \left(\frac{\partial^\gamma}{\partial x^\gamma} \phi_x(x, z+a) \right)^2 + \left(\frac{\partial^\gamma}{\partial x^\gamma} \phi_z(x, z+a) \right)^2. \quad (8)$$

In the classical use of the analytic signal, one considers the modulus of the analytic signal but the interpretation of its phase is missing. Recent improvements are due to the interpretation of the phase [Smith et al., 1998]. Within the theory of continuous wavelet transforms [Holschneider, 1995] the use of both the modulus and phase (and both the real and imaginary parts) of the upward continued analytic signal at different levels (complex wavelet coefficients for different dilations) is natural and allows interesting properties regarding the geometry of the singularities to be taken into account.

Besides, the exponent β defined in (3) depends on the derivative order γ and the homogeneity degree of the

source α . Thus it relates to the structural index N used in Euler deconvolution which is also based upon an homogeneity property, that of the field [Thompson, 1982; Reid et al., 1990; Huang, 1996]. Using Euler deconvolution, the structural index N must be assumed a priori, except when applied in conjunction with other procedures [Huang, 1996; Ravat and Taylor, 1998; Barbosa et al., 1999]. Using wavelets, the homogeneity degree of the source α can be determined from the scaling exponent β without a priori value. Hereafter, we give the exponent β of the 1-D wavelet coefficients as a function of α . We also give the homogeneity degree of the associated magnetic potential $-N$ in different situations, depending on the type of anomaly field or potential ϕ which is analyzed:

V (gravity potential, or Green's function),

$$\beta_V = -\gamma + \alpha + 2 = -(\gamma + N - 1);$$

$g = \nabla V$ (gravity field) or $U = -\nabla V.M$ (magnetic potential due to the dipole M),

$$\beta_g = \beta_U = -\gamma + \alpha + 1 = -(\gamma + N);$$

$T = -\nabla U$ (magnetic field) or $\partial_z g$ (vertical derivative of the gravity field),

$$\beta_T = -\gamma + \alpha = -(\gamma + N + 1).$$

Classically, one defines N from the potential field but this gives a value which depends on the analyzed data,

and this involves a shift of 1 between the gravity and magnetic cases. Instead, we consider its definition given by Huang [1996]; this is more reliable as it gives a value which depends only on the geometry of the source: N is the opposite to the homogeneity degree of the magnetic potential and is also that of the corresponding gravity field.

3. Synthetic Examples

3.1. Total Magnetic Field Anomaly in Profiles

We consider the magnetic total field anomaly produced by a set of elementary magnetization vectors with declination D and inclination I within a normal field of declination D_n and inclination I_n . To clarify the analytic expressions in the case of profiles, we use two simplifications. First, when profiles are striking geographic north with an angle φ and perpendicular to the sources (Figure 4), one can introduce an apparent inclination I' and an apparent normal field inclination I'_n corresponding to a geomagnetic south-north profile [de Gery and Naudy, 1957]:

$$\tan I' = \frac{\tan I}{\cos(D + \varphi)}, \quad \tan I'_n = \frac{\tan I_n}{\cos(D_n + \varphi)}. \quad (9)$$

Second, one can consider magnetization vectors with declination D and inclination I equal to those of the normal field D_n and I_n , respectively, as if there were only induced magnetization. In this case, apparent inclinations are equal ($I' = I'_n$).

Hence the total magnetic field anomaly δT at (x, z) is given by two conjugated symmetrical and antisymmetrical functions δT_1 and δT_2 associated with second-order derivatives of the Green's function V (see detailed expressions in Appendix A):

$$\delta T = \left(\frac{\sin I}{\sin I'} \right)^2 (-\delta T_1 \cos 2I' + \delta T_2 \sin 2I'); \quad (10)$$

δT_1 is equal to the anomaly field reduced to the pole ($I' = 90^\circ$), and δT_2 is equal to the anomaly field reduced to the inclination $I' = 45^\circ$. Analytic expressions for the total field anomaly due to a given body are equivalent to those of south-north profiles by replacing inclinations I with apparent inclinations I' (for a collection of analytic expressions, see Telford et al. [1990]).

In this paper, calculations of the wavelet coefficients will be done by taking derivatives (from equations (5), and (7)). It can be shown that the modulus of the real and imaginary parts exhibit extrema controlled by the derivative order γ and the mean apparent inclination $\mathfrak{S} = (I' + I'_n)/2$, while the modulus of the complex coefficients exhibit extrema whose geometry is independent of the mean apparent inclinations (Appendix B). A special formulation for extended sources and the corresponding complex wavelet coefficients is possible using the complex variables method; it is introduced in Appendix C for its potential applications in the numerical approach to the direct and inverse problems. We have calculated analytical expressions for some typical simple 2-D bodies below. For local sources at depth z_0 , exact power laws of $(a + z_0)$ are shown (a is the dilation, or continuation altitude); for extended sources, Taylor expansions are calculated to analyze the perturbation due to a finite extent.

3.2. Local Elementary Magnetization

As a first synthetic case, let us consider the magnetic total field anomaly produced at level z (positive downward) by a local elementary magnetization vector located at (x_0, z_0) . For this elementary magnetization,

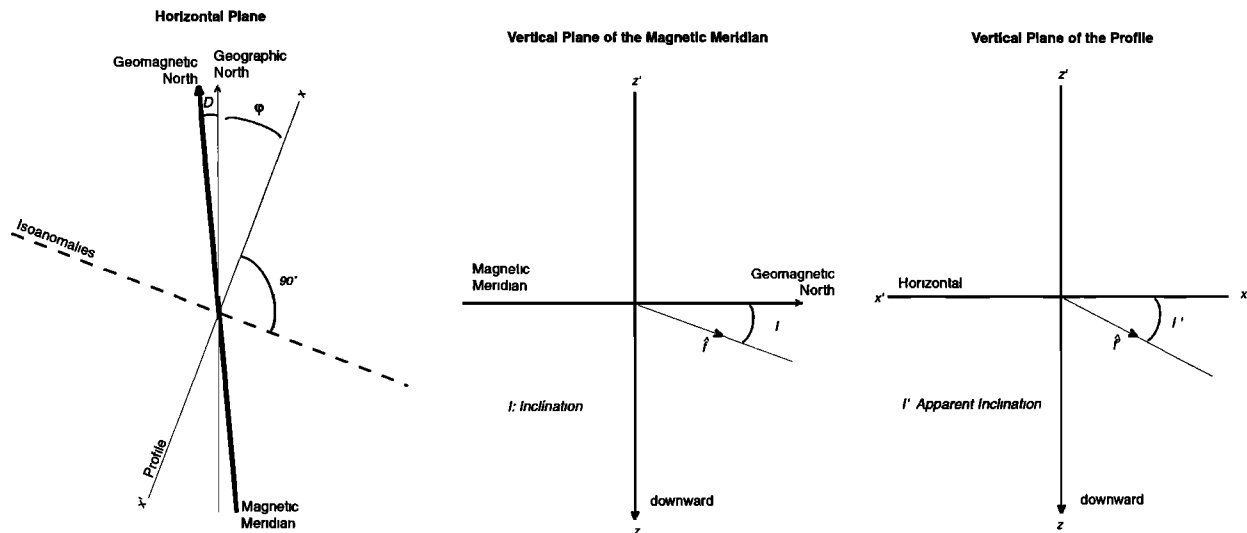


Figure 4. Apparent inclination I' versus inclination I : The unit vector \hat{f} (respective \hat{f}_n) defining the direction of the magnetization M (respective of the magnetic field F) gives the apparent inclination I' (respective I'_n) when projected onto the vertical plane of the profile.

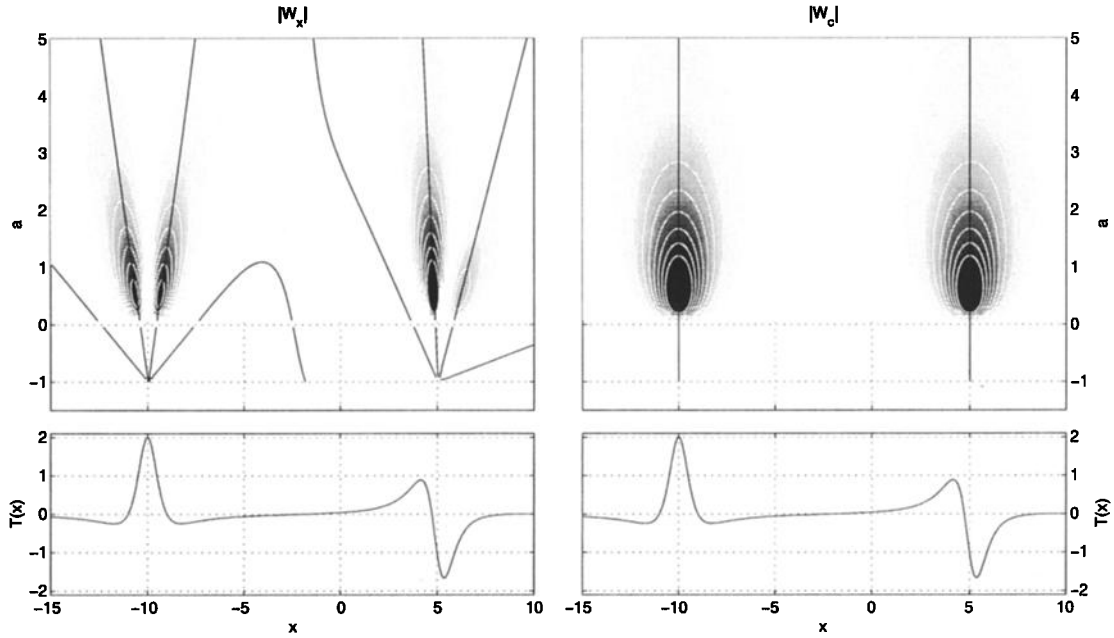


Figure 5. Local elementary magnetizations at depth $z_0 = 1$ (and $a = -z_0 = -1$) with apparent inclinations $I' = 90^\circ$ at $x = -10$ and $I' = 29.16^\circ$ at $x = +5$: (bottom) Total magnetic field, and (left) modulus of real wavelet coefficients or (right) complex wavelet coefficients. Isovalues are shown in white with regular intervals. Modulus maxima lines are shown in black with their downward continuation to the source.

which is concentrated on an infinite horizontal line, the Green's function is $V(x, z) = \ln[(x - x_0)^2 + (z_0 - z)^2]$; so (10) holds with

$$\begin{aligned} \delta T_1(x, z) &= -2 \frac{(x - x_0)^2 - (z_0 - z)^2}{[(x - x_0)^2 + (z_0 - z)^2]^2}, \\ \delta T_2(x, z) &= -4 \frac{(x - x_0)(z_0 - z)}{[(x - x_0)^2 + (z_0 - z)^2]^2}. \end{aligned} \quad (11)$$

Thus using variables $X = x - x_0$ and $Z = z_0 - z = z_0 + a$ and prefactor $K = 4(\sin I / \sin I')^2$, one gets the following wavelet coefficients:

$$\mathcal{W}_{\psi_2|\delta T(\cdot, z=0)}(x, a) = -Ka e^{-i2I'} (X + iZ)^{-3}. \quad (12)$$

We have computed these wavelet coefficients for two orientations of magnetization: in a south-north profile at the pole ($I' = 90^\circ$) where the anomaly is symmetrical and in the SSW-NNE profiles of the Guiana survey ($I' = 29.16^\circ$). Figure 5 shows these wavelet coefficients. Extrema lines of the real wavelet coefficients intersect at the point $(x_0, a = -z_0)$ inside the lower half plane. There is only one modulus maxima line of the complex wavelet coefficients (with equation $x = x_0$).

Wavelet coefficients for any derivative order $\gamma \in \mathbb{N}^*$ read for $x = x_0$:

$$\mathcal{W}_{\psi_2|\delta T(\cdot, z=0)}(x_0, a) = 2(\gamma + 1)! \left(\frac{\sin I}{\sin I'}\right)^2 \frac{a^\gamma e^{i(-2I' + (\gamma+2)\frac{\pi}{2})}}{(z_0 + a)^{\gamma+2}}. \quad (13)$$

When the depth z_0 is known, modulus $|W|$ and phase Φ along a modulus maxima line simply give the values of the homogeneity degree $\alpha = -2$ and the apparent inclination $I' = -\Phi/2 + (\gamma + 2)(\pi/4)$ (modulo π).

When the depth z_0 is unknown, adjusting a straight line to the plots of $\log |W|^\gamma / a^\gamma$ versus $\log(z_0 + a)$ for a set of a priori depths z_0 and looking for the best least squares fit provides both z_0 and α (Figure 6).

3.3. Local Multipole Magnetization

As a second synthetic case, let us consider a multipole magnetization vector located at (x_0, z_0) which is formally an oblique derivative of the local elementary magnetization vector previously analyzed. Asymptotic expansions of the far field due to extended sources imply the sums of multipoles. For instance, an elementary pole plus a dipole mass can be used as a model for an inclined gravimetric border [Moreau, 1995]. Let us call θ_1 the direction of the oblique derivative corresponding to the dipole magnetization vector. Then θ_2 is the direction of the second oblique derivative corresponding to the quadrupole magnetization vector, and θ_n is the direction of the n th oblique derivative corresponding to the n th-multipole magnetization vector. We assume that the structure of this multipole source is still infinite in the horizontal direction perpendicular to the profile, so that θ angles have to be considered in the vertical plane of the profile (apparent angles θ' are equal to θ). Then for this n th-multipole magnetization, n additional oblique derivatives (in directions θ_j for $1 \leq j \leq n$) have to be performed in (10), (12), and (13).

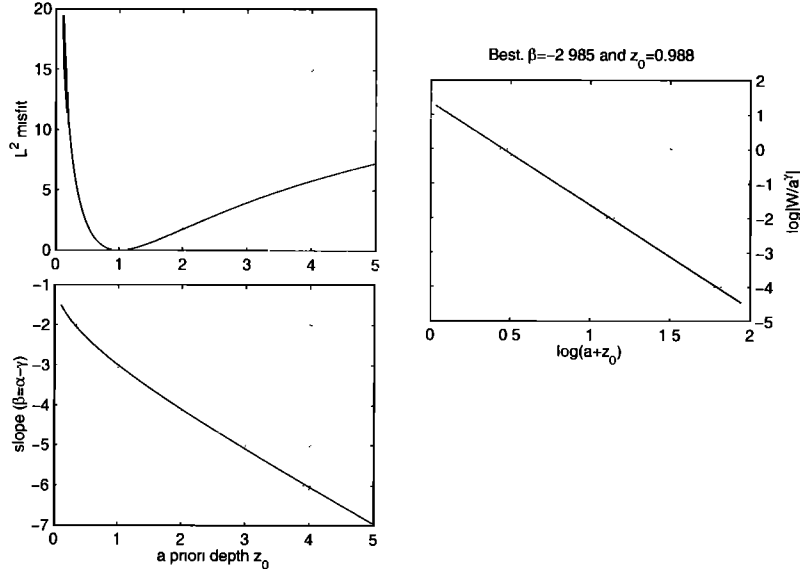


Figure 6. From the wavelet coefficients of Figure 5, (right) computation of the best slope β and depth z_0 is accomplished by least squares linear regressions of $\log(|W_a|/a^\gamma)$ versus $\log(a + z_0)$. (left) A set of a priori depths $[0.1, 5]$ has been tested; this gives good estimates for both homogeneity degree $\alpha = \beta + \gamma = -1.985$ and depth $z_0 = 0.988$.

Thus using variables $X = x - x_0$ and $Z = z_0 - z = z_0 + a$, prefactor $K = 12(\sin I / \sin I')^2$, and angle $\xi = -2I' - \theta_1$, one gets the following wavelet coefficients for the dipole magnetization source in direction θ_1 :

$$\mathcal{W}_{\psi_c^1|\delta T^1(\cdot, z=0)}(x, a) = Ka e^{i\xi} (X + iZ)^{-4}. \quad (14)$$

We have also calculated the wavelet coefficients for any derivative order $\gamma \in \mathbb{N}^*$ and any multipole degree $n \in \mathbb{N}$, which reads for $x = x_0$,

$$\mathcal{W}_{\psi_c^\gamma|\delta T^n(\cdot, z=0)}(x_0, a) = 2(\gamma + n + 1)! \left(\frac{\sin I}{\sin I'}\right)^2 \frac{a^\gamma e^{i(-2I' - \Theta_n + (\gamma + n + 2)\frac{\pi}{2})}}{(z_0 + a)^{\gamma + n + 2}}, \quad (15)$$

where $\Theta_n = \sum_{j=1}^n \theta_j$ characterizes the combination of directions in this multipole magnetization.

Again, there is only one modulus maximum line of the complex wavelet coefficients (with equation $x = x_0$). The modulus $|\mathcal{W}|$ and phase Φ along this maximum line simply give the values of the homogeneity degree $\alpha = -(n + 2)$ and either the apparent inclination $I' = -(\Phi + \Theta_n)/2 + (\gamma - \alpha)\pi/4$ (modulo π), or the sum of directions $\Theta_n = -\Phi - 2I' + (\gamma - \alpha)\pi/2$ (modulo 2π).

3.4. Magnetization Step

As a first example of a nonlocal source, let us consider the total field anomaly generated by a vertical step located at x_0 and depths $[z_1, z_2]$ (with height $h = z_2 - z_1$) of elementary magnetization with normal apparent inclination I' (source on the north, for $x \geq x_0$). Equation (10) holds with

$$\begin{aligned} \delta T_1(x, z) &= 2 \left(\tan^{-1} \frac{z_2 - z}{x - x_0} - \tan^{-1} \frac{z_1 - z}{x - x_0} \right) \\ \delta T_2(x, z) &= \ln \frac{(x - x_0)^2 + (z - z_2)^2}{(x - x_0)^2 + (z - z_1)^2}. \end{aligned} \quad (16)$$

Thus, using variables $X = x - x_0$, $Z_1 = z_1 - z = z_1 + a$, and $Z_2 = z_2 - z = z_2 + a$ and prefactor $K = 2(\sin I / \sin I')^2$, one gets the following wavelet coefficients for the vertical step:

$$\mathcal{W}_{\psi_c^1|\delta T(\cdot, z=0)}(x, a) = Ka e^{-i2I'} \left[\frac{1}{Z_2 - iX} - \frac{1}{Z_1 - iX} \right]. \quad (17)$$

Figure 7 shows these wavelet coefficients. The shape of modulus maxima lines for real wavelets is not as simple as for a local source (in section 3.2). For small dilations a , these are not straight but converge at about the top of the step source; for dilations a which are large enough (typically $(z_0 + a) \gg h/2$), these are straight lines and converge at about the mean depth of the step $z_0 = (z_2 + z_1)/2$, as if the source was local.

The argument and modulus are

$$\begin{aligned} \Phi_{\psi_c^1|\delta T(\cdot, z=0)}(x, a) &= -2I' + \pi + \tan^{-1} \frac{X}{Z_1} + \tan^{-1} \frac{X}{Z_2}, \\ |\mathcal{W}_{\psi_c^1|\delta T(\cdot, z=0)}(x, a)| &= \frac{Kab}{\sqrt{(X^2 + Z_1^2)(X^2 + Z_2^2)}}. \end{aligned} \quad (18)$$

Equations (18) show that there is only one modulus maximum line (for which $\partial_x |\mathcal{W}_{\psi_c^1}(x, a)|$ is zero), defined by $X = 0$ (vertical to the step source, at $x = x_0$). Thus, when we consider modulus from neither the real nor imaginary part ($|\mathcal{W}_{\psi_x^1}|$ nor $|\mathcal{W}_{\psi_y^1}|$) but rather from the complex coefficient itself ($|\mathcal{W}_{\psi_c^1}|$), there is one single

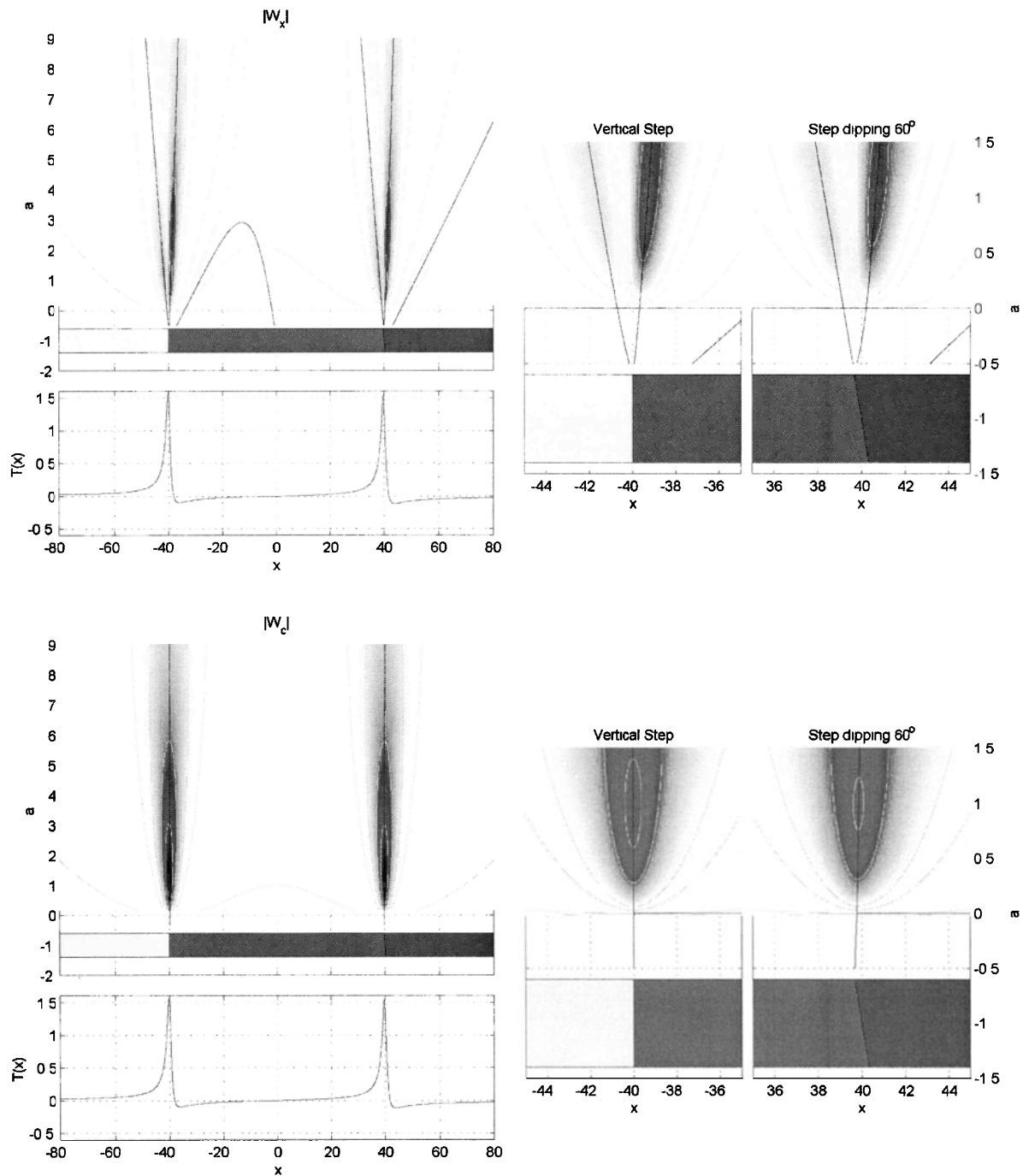


Figure 7. Vertical and dipping steps of magnetization (at mean depth $z_0 = 1$, with apparent inclination $I' = 29.16^\circ$): (bottom left) Total magnetic field, and (top left) corresponding modulus of real or complex wavelet coefficients (zoomed at right). Isovalues are shown shaded with regular intervals. Modulus maxima lines are shown in black; their continuation to the source is shown in the lower half-space (analytically, above the top of the source).

modulus maximum line which is straight and vertical (a well-known property for the maximum of the analytic signal). The phase along this maximum line equals $\pi - 2I'$:

$$\mathcal{W}_{\psi_2}|\delta T(.,z=0)(x_0, a) = 2 \left(\frac{\sin I'}{\sin I'} \right)^2 \frac{ah e^{i(-2I'+\pi)}}{(z_1 + a)(z_2 + a)}. \tag{19}$$

Asymptotic behavior is obtained with a Taylor expansion for $z_0 + a \gg h/2$ (large dilations or large average depth):

$$\mathcal{W}_{\psi_2}|\delta T(.,z=0)(x_0, a) \simeq 2 \left(\frac{\sin I'}{\sin I'} \right)^2 a h e^{i(-2I'+\pi)} \left[\frac{1}{(z_0+a)^2} + \frac{(h/2)^2}{(z_0+a)^4} \right]. \tag{20}$$

The first-order term is that of a local source located at depth z_0 ; its homogeneity degree, given by the scaling exponent $\beta = -2$, is $\alpha = -1$ (that of a step source whose structural index is known to be $N = -(\alpha + 1) = 0$). The second-order term is a perturbation (of $100 \times [(h/2)/(z_0 + a)]^2$ %), this is another local source located at depth z_0 but with homogeneity degree $\alpha = -3$ (dipole of magnetization).

Thus (17) to (20) do not only provide the mean depth z_0 (at the convergence of modulus extrema lines of real wavelet coefficients), the apparent inclination I' (from the phase of the complex wavelet coefficients) and the characteristic homogeneity degree $\alpha = -1$ using the slope β in the plot of $\log(|\mathcal{W}_a|/a)$ versus $\log(a + z_0)$ (along modulus extrema lines), but they also provide a way to estimate the height h of the step from residuals in the determination of β .

Indeed, moduli of (20) may be first approximated in a form valid for very large dilations:

$$\ln \frac{|\mathcal{W}_{\psi_2^{\frac{1}{2}}|\delta T(\cdot, z=0)}(x_0, a)|}{a} \simeq k + \beta \ln(z_0 + a). \quad (21)$$

Fitting a straight line to this approximation provides the slope $\beta = \alpha - 1$ and the log factor $k = \ln(Kh)$ (where K is the prefactor used in (17) which includes information on I, I' and the intensity of magnetization). These then can be used to plot the following function $H(a)$ which converges rapidly to a limit which is the height h of the step (see Figure 8):

$$H(a) \simeq 2(z_0 + a) \left| \ln \frac{|\mathcal{W}_{\psi_2^{\frac{1}{2}}|\delta T(\cdot, z=0)}(x_0, a)|}{a} - k - \beta \ln(z_0 + a) \right|^{\frac{1}{2}}. \quad (22)$$

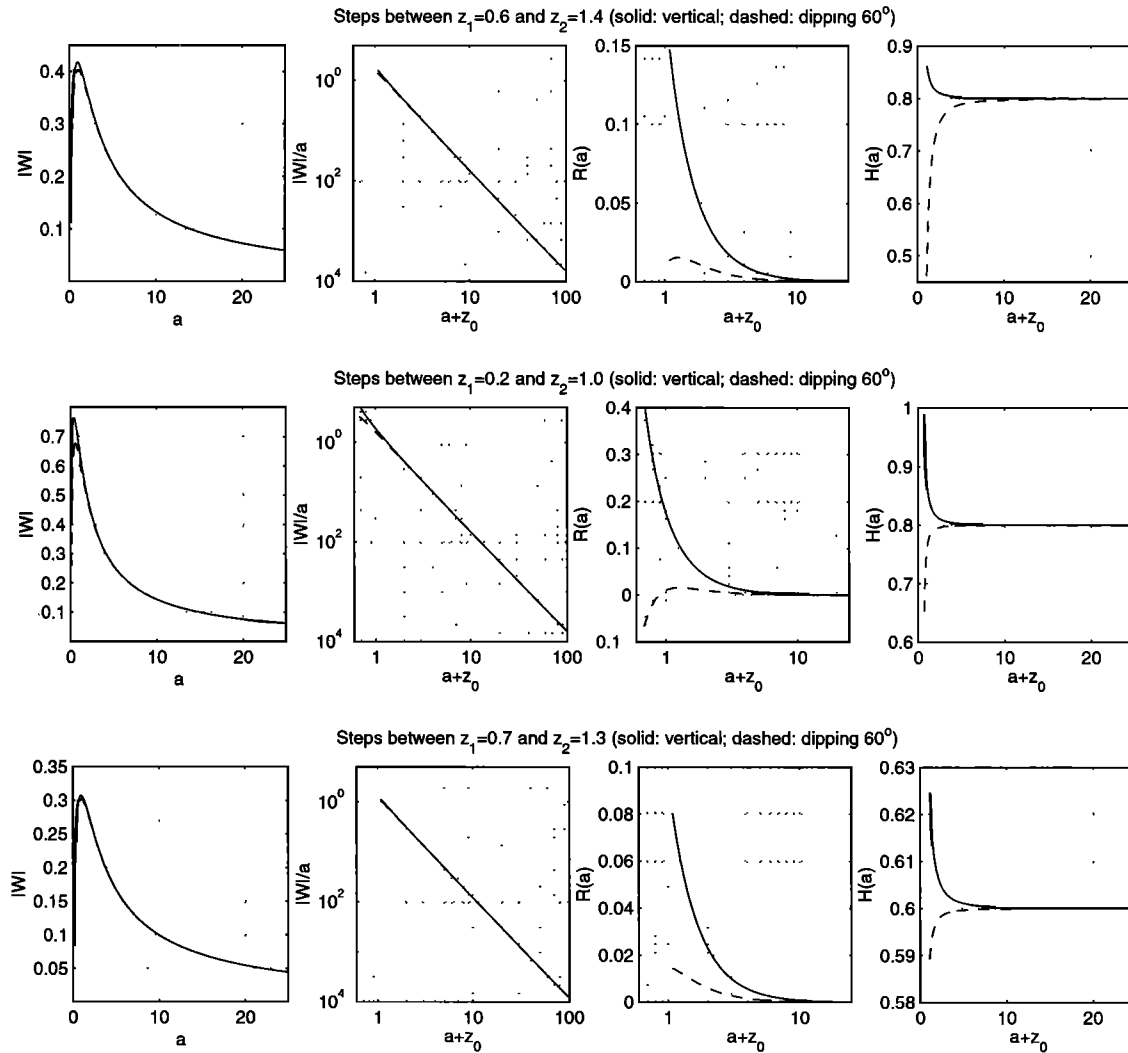


Figure 8. Scaling relations for vertical and dipping ($\theta = -40^\circ$) steps of magnetization (with apparent inclination $I' = 29.16^\circ$). (left to right) Modulus of complex wavelet coefficients along $x = x_0$, first-order scaling (equation (25)), residual due to the second-order term (equation (31)), and function $H(a)$ estimating the height of the step (equation (32)). Correspond to (top) anomaly in Figure 7 ($z_0 = 1, h = 0.8$), (middle) to a lower depth ($z_0 = 0.6, h = 0.8$), and (bottom) to a lower height ($z_0 = 1, h = 0.6$).

Let us now consider an inclined step with dip angle $\pi/2 - \theta$: with a limit between the two points (x_1, z_1) and (x_2, z_2) and middle point at $x_0 = (x_1 + x_2)/2$ and $z_0 = (z_1 + z_2)/2$. Similar algebraic manipulations as those used for the vertical step allow us to calculate the total field anomaly and its derivatives.

Using variables $X_1 = x - x_1$, $X_2 = x - x_2$, $Z_1 = z_1 - z = z_1 + a$, and $Z_2 = z_2 - z = z_2 + a$; prefactor $K = 2(\sin I/\sin I')^2$; and angle $\xi = -2I' + \theta$, one gets the wavelet coefficients for the inclined step (to be compared with (17)):

$$\mathcal{W}_{\psi_c^1|\delta T(\cdot, z=0)}(x, a) = Ka \cos \theta e^{i\xi} \left[\frac{1}{Z_2 - iX_2} - \frac{1}{Z_1 - iX_1} \right]. \quad (23)$$

The argument and modulus can be written, generalizing equations (18), respectively, as follows:

$$\Phi_{\psi^1|\delta T(\cdot, z=0)}(x, a) = -2I' + \pi + \tan^{-1} \frac{X_1}{Z_1} + \tan^{-1} \frac{X_2}{Z_2},$$

$$|\mathcal{W}_{\psi_c^1|\delta T(\cdot, z=0)}(x, a)| = \frac{Kah}{\sqrt{(X_1^2 + Z_1^2)(X_2^2 + Z_2^2)}}. \quad (24)$$

Solving for $\partial|\mathcal{W}_{\psi_c^1}(x, a)|/\partial x = 0$ implies that modulus maxima are defined by solutions of a second-order polynomial in $Z = z - z_0$ (and fourth-order in $X = x - x_0$): with $\nu = X/(h/2) \neq 0$ (and $\theta \neq 0$). Solutions are

$$a = -z_0 + \frac{h}{2\nu} \tan \theta \left(1 \pm \sqrt{(1 + \nu^2)(1 - \nu^2 \cot^2 \theta)} \right). \quad (25)$$

Equation (25) tells us that for different dip angles $\pi/2 - \theta$, the modulus maximum line is not a straight line and its slope depends on the dilation a and more precisely on $(a + z_0)/(h/2)$, ν , and θ . It is possible to make a Taylor expansion of this equation near to the vertical of the source (for $\nu \ll 1$); this gives two types of asymptotic behavior. For large dilations a (for $a + z_0 \gg h/2$) the maximum line is a branch of a hyperbola whose asymptote is $x = x_0$. For small dilations the maximum line is a branch of a polynomial in $x - x_0$ whose first order corresponds to a straight line with slope $\cot(2\theta)$:

If $a + z_0 \gg h/2$

$$a + z_0 \simeq \frac{2(h/2)^2 \tan \theta}{x - x_0} + O(x - x_0);$$

Otherwise

$$a + z_0 \simeq -(x - x_0) \cot(2\theta) \left[1 + \frac{\nu^2}{4} \frac{(\cot^2 \theta + 1)^2}{\cot^2 \theta - 1} + O(\nu^4) \right]. \quad (26)$$

This quantifies a classical property of potential field anomalies over a dipping homogeneous source: At low altitude the main contribution is due to the upper part of the source; while at increasing altitude the relative contribution of deeper parts progressively increases and the location of the maximum effect moves to the vertical passing through the ‘‘center of gravity’’ of the source.

Writing wavelet coefficients along modulus maxima similarly to (19) for a vertical step, then Taylor expanding for $z_0 + a \gg h/2$ (large dilations or large average depth) gives

$$|\mathcal{W}_{\psi_c^1|\delta T(\cdot, z=0)}(x, a)| \simeq 2 \left(\frac{\sin I}{\sin I'} \right)^2 ah \left[\frac{1}{(z_0 + a)^2} + (1 - \tan^2 \theta) \frac{(h/2)^2}{(z_0 + a)^4} \right]. \quad (27)$$

Thus, scaling parameters at large dilations are those of the vertical step (equation (20)) except for the relative amplitudes between terms of the Taylor expansion which depend on the dip angle $\pi/2 - \theta$.

Fitting a straight line as in (21) provides the slope $\beta = \alpha - 1$ and the log factor $k = \ln(Kh)$. These can then be used, along the extrema lines, to plot a function $H(a)$ similar to that defined by (22), which converges for $\theta \neq \pm\pi/4$ to a limit which is the height h of the step (see Figure 8):

$$H(a) \simeq \frac{2(z_0 + a)}{|1 - \tan^2 \theta|^{\frac{1}{2}}} \cdot \left| \ln \frac{|\mathcal{W}_{\psi_c^1|\delta T(\cdot, z=0)}(x_0, a)|}{a} - k - \beta \ln(z_0 + a) \right|^{\frac{1}{2}}. \quad (28)$$

The phase is $\pi - 2I'$ for large dilations and could be used to determine an unknown inclination I' .

Note that the search for the height from (22) or (28) assumes that one has first determined the dip angle $\pi/2 - \theta$: This could be done via the direction of the modulus maxima lines (see equation (25)). When the angle remains unknown, an estimation from equation (22) instead of (28) would be useful anyway as it gives the correct height within a factor of 2 for any θ value except for values of about 45° or 90° . Other possible errors are due to the uncertainty in x location and modulus maximum determination, which are involved in the Taylor expansion along the modulus maximum line. Quantification of this remark is given by manipulations showing that the next term in the expansion of (20) is $-(x - x_0)^2/(z_0 + a)^4$, so that $H(a)$ may give an average value of $\sqrt{h^2 - 4(x - x_0)^2}$ instead of the height h itself (noise in positioning or continuation also leads to errors in the wavelet coefficients).

3.5. Magnetization Strip

Let us now consider the total field anomaly generated by an inclined strip with dip angle $\pi/2 - \theta$: with a limit between the two points (x_1, z_1) and (x_2, z_2) and middle point at $x_0 = (x_1 + x_2)/2$ and $z_0 = (z_1 + z_2)/2$. This strip is formally the horizontal derivative of a right step source. So, as shown by *Moreau et al.* [1999], its wavelet coefficients can be obtained by a simple horizontal derivative of (23): The wavelet coefficients of order γ for the strip are those of order $\gamma + 1$ for the right step divided by a dilation factor a . Note that a

calculation based upon (10) as done in sections 3.1-3.4 would imply the same results.

Thus using variables $X_1 = x - x_1$, $X_2 = x - x_2$, $Z_1 = z_1 - z = z_1 + a$, and $Z_2 = z_2 - z = z_2 + a$; prefactor $K = 4(\sin I / \sin I')^2$; angle $\xi = -2I' + \theta$; and the height $h = z_2 - z_1$, the wavelet coefficients read

$$\mathcal{W}_{\psi_c^1|\delta T(\cdot, z=0)}(x, a) = Ka \cos \theta e^{i\xi} \left[\frac{i}{(Z_2 - iX_2)^2} - \frac{i}{(Z_1 - iX_1)^2} \right]. \quad (29)$$

The shape of modulus maximum lines of these wavelet coefficients (not shown) is similar to that of the step source (Figure 7). With real wavelets they converge either to the top of the strip or to its mean depth z_0 .

While analytical formulation of modulus maxima of complex wavelet coefficients for the inclined step are solutions of a second order polynomial in $Z = z - z_0$ (equations (25) and (26)), the strip case implies a fifth-order polynomial which does not simplify easily. Nevertheless, graphical solutions for modulus maxima (plotted as zeros of x derivatives of complex wavelet moduli) are accessible, showing asymptotic behavior similar to that obtained for the step source (Figure 7).

In the case of a vertical strip, analytical formulations are possible: Complex wavelet coefficients on modulus maxima lines (for $x = x_0$) obey

$$\mathcal{W}_{\psi_c^1|\delta T(\cdot, z=0)}(x_0, a) = 2 \left(\frac{\sin I}{\sin I'} \right)^2 \frac{a(z_2^2 - z_1^2) e^{i(-2I' + 3\frac{\pi}{2})}}{(z_1 + a)^2(z_2 + a)^2}. \quad (30)$$

Calling h the height of the strip and z_0 its mean depth, we obtain the following Taylor expansion for $z_0 + a \gg h/2$ (large dilations or large average depth):

$$\mathcal{W}_{\psi_c^1|\delta T(\cdot, z=0)}(x_0, a) \simeq 4 \left(\frac{\sin I}{\sin I'} \right)^2 a h e^{i(-2I' + 3\frac{\pi}{2})} \left[\frac{1}{(z_0 + a)^3} + 2 \frac{(h/2)^2}{(z_0 + a)^5} \right]. \quad (31)$$

This is similar to (20) except for a factor 2 and for the powers of $(z_0 + a)$. The same estimation technique as that shown for the vertical step applies: Equations (21) and (22) now apply with $\beta = \alpha - \gamma = -3$. Here, the first-order term is that of an elementary local magnetization (of homogeneity $\alpha = -2$), which characterizes how the strip transforms into a horizontal line for h small.

Similarities between the vertical step and strip cases also apply for both inclined cases in Taylor expansions along modulus maxima lines, so that a function $H(a)$ similar to that defined in (22) and (28), which converges (for almost all dipping angles θ) to a limit which is the height h , exists:

$$H(a) \simeq 2(z_0 + a)f(\theta) \cdot \left| \ln \frac{|\mathcal{W}_{\psi_c^1|\delta T(\cdot, z=0)}(x_0, a)|}{a} - k - \beta \ln(z_0 + a) \right|^{\frac{1}{2}}, \quad (32)$$

where $k = \ln(Kh)$ and $f(\theta) = (2|1 - \tan^2 \theta|)^{-\frac{1}{2}}$. Along modulus maximum lines, phases for large dilation a converge to $-2I' + 3\pi/2$, which is the value for an elementary local magnetization (again, this characterizes how the strip transforms into a horizontal line for h small).

3.6. Magnetization Prism

As a final synthetic case, let us consider the total field anomaly generated by an inclined prism whose limits are the four points (x_1, z_1) , (x_2, z_2) , (x_3, z_3) , and (x_4, z_4) (clockwise, with $z_1 = z_4$, $z_2 = z_3$, and $x_1 - x_4 = x_2 - x_3$). The dip angle is $\pi/2 - \theta$, the height is $h = z_2 - z_1$, and the horizontal length is $l = x_1 - x_4$. As (x_1, z_1) , (x_2, z_2) define the right edge and (x_3, z_3) , (x_4, z_4) define the left edge (Figure 9), analytic expressions for the wavelet coefficients are given by the difference between wavelet coefficients of two step sources.

Using variables $X_{01} = x - x_1 + l/2$, $X_{02} = x - x_2 + l/2$, $Z_1 = z_1 - z = z_1 + a$, and $Z_2 = z_2 - z = z_2 + a$; prefactor $K = 2(\sin I / \sin I')^2$; and angle $\xi = -2I' + \theta$, one gets the wavelet coefficients for the inclined prism (to be compared with equation (23)):

$$\mathcal{W}_{\psi_c^1|\delta T(\cdot, z=0)}(x, a) = Ka \cos \theta e^{i\xi} \left[\frac{1}{Z_2 - i(X_{02} + l/2)} - \frac{1}{Z_1 - i(X_{01} + l/2)} - \frac{1}{Z_2 - i(X_{02} - l/2)} + \frac{1}{Z_1 - i(X_{01} - l/2)} \right]. \quad (33)$$

For small length l (for $l \ll h$) this corresponds to the horizontal derivative of the inclined step, so that we recover the strip. Thus one expects the same kind of results as those obtained for the strip. As shown on Figure 9, properties of the wavelet coefficients such as the homogeneity degree are the same as for the strip. These are properties corresponding to the asymptotic expansions for large dilations a . Nevertheless, for small dilations (for $z_0 + a \sim l/2$), modulus extrema lines and isoarguments exhibit branching; they point toward two top edges (step sources) instead of one single edge obtained from the strip source.

For clarity, exact analytical expressions of complex wavelet coefficients on modulus maximum lines are given only for the vertical prism (at $x = x_0$):

$$\mathcal{W}_{\psi_c^1|\delta T(\cdot, z=0)}(x_0, a) = 2 \left(\frac{\sin I}{\sin I'} \right)^2 a l h \frac{(z_1 + z_2 + 2a) e^{i(-2I' + 3\frac{\pi}{2})}}{[(z_1 + a)^2 + (\frac{l}{2})^2] [(z_2 + a)^2 + (\frac{l}{2})^2]}. \quad (34)$$

Calling z_0 the mean depth, we obtain the following Taylor expansion for $z_0 + a \gg h/2$, $z_0 + a \gg l/2$ (large dilations or large average depth) and $h\sqrt{|1 - \tan^2 \theta|} \neq l$:

$$\mathcal{W}_{\psi_c^1|\delta T(\cdot, z=0)}(x_0, a) \simeq 4 \left(\frac{\sin I}{\sin I'} \right)^2 a l h \cdot e^{i(-2I' + 3\frac{\pi}{2})} \left[\frac{1}{(z_0 + a)^3} + 2 \frac{(h/2)^2 \sec^2 \theta \cos 2\theta - (l/2)^2}{(z_0 + a)^5} \right]. \quad (35)$$

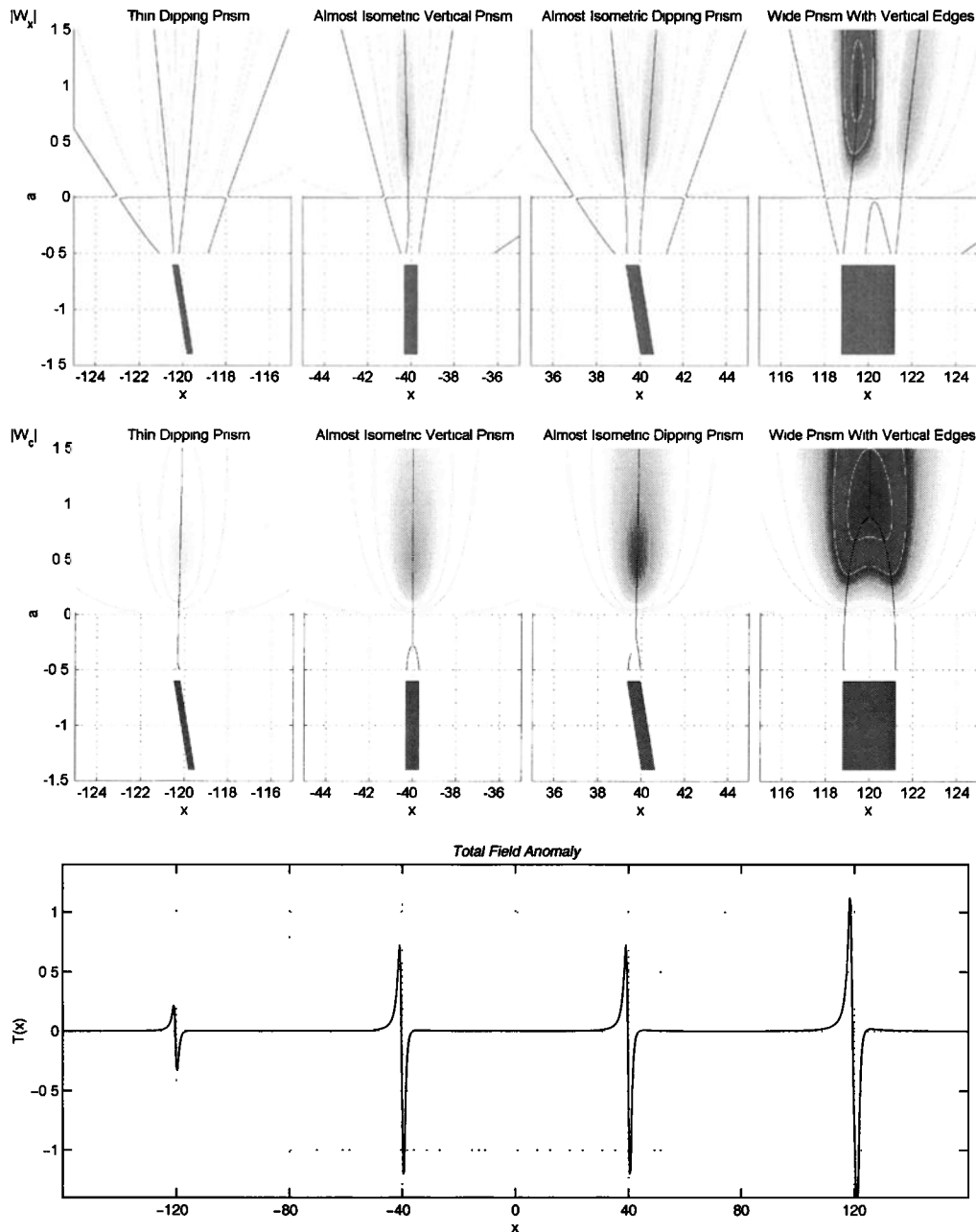


Figure 9. Vertical and dipping ($\theta = -40^\circ$) prisms of magnetization (at depth $z_0 = 1$, with apparent inclination $I' = 29.16^\circ$): (bottom) Total magnetic field and corresponding modulus of (top) real or (middle) complex wavelet coefficients. Isovalues are shown shaded with regular intervals. Modulus maxima lines are shown in black; their continuation down to the source is shown for small dilations in the lower half-space.

This is similar to (31) except for prefactor l and additional term in l^2 : The first is linked to the change in the source density (per volume instead of per surface) which is hidden for the calculations; the second is due to the change in source geometry. It is difficult to interpret the prefactors except in cases of well-known a priori source density where conventional techniques apply. Nevertheless, it is worth using a multiscale technique based upon the multipole expansion to obtain estimates for depth and source extensions. There exists a function

$H(a)$ similar to that defined in (32), which converges (for almost all dip angles $\pi/2 - \theta$) to a limit which is the height h of the prism:

$$H(a) \simeq 2(z_0 + a)f(\theta, \frac{l}{h}) \cdot \left| \ln \frac{|\mathcal{W}_{\psi_2^1} \delta T(\cdot, z=0)(x_0, a)|}{a} - k - \beta \ln(z_0 + a) \right|^{\frac{1}{2}}, \quad (36)$$

where $k = \log(2Klh)$, $\beta = -3$, and $f(\theta, l/h) = (2|1 - \tan^2 \theta - (l/h)^2|)^{-0.5}$ is a factor which depends on the

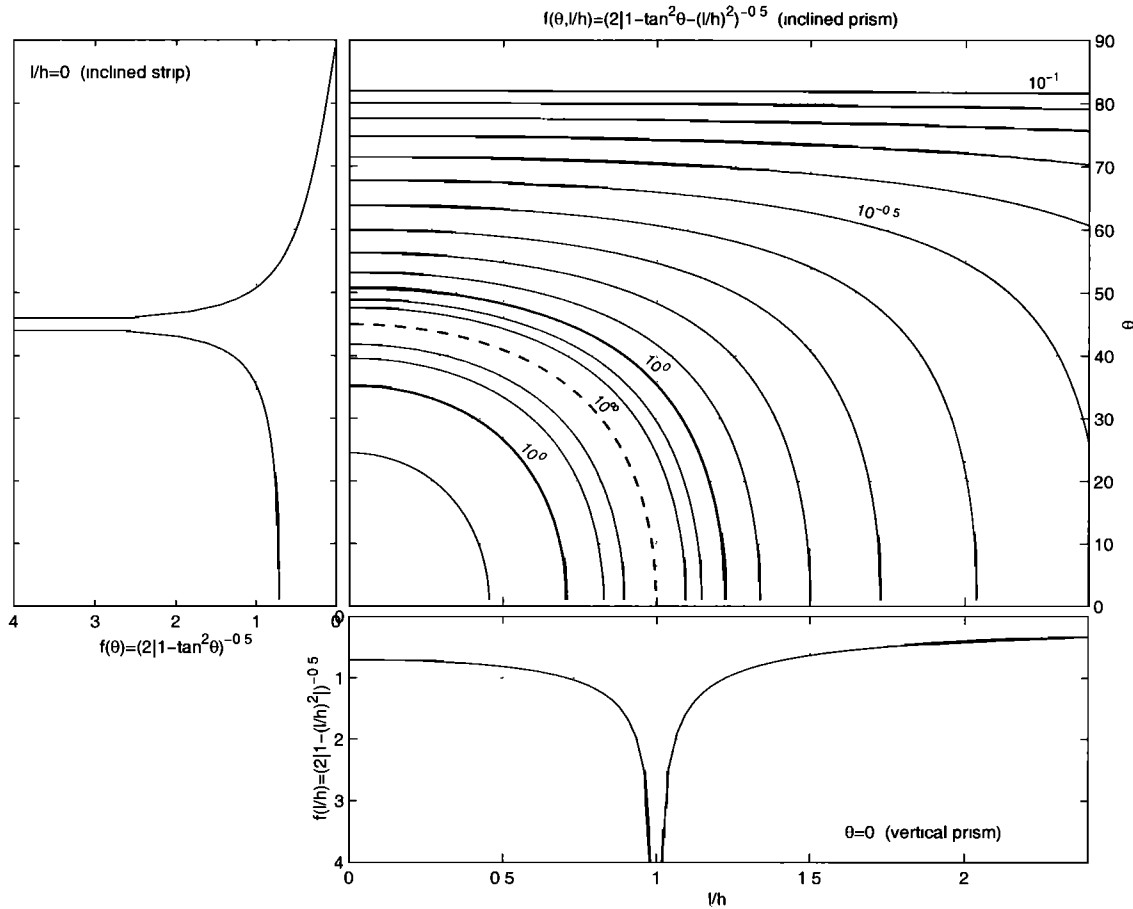


Figure 10. Multiplicative correction factor $f(\theta, l/h)$ for strip and prism to be applied to the height estimator defined in equation (26) (undefined in the dashed curve neighborhood).

ratio between l and h and equals $1/\sqrt{2}$ for $\theta = 0$ and $l \ll h$ (see Figure 10).

Along modulus maxima line, phases for large dilation a converge to $-2I' + 3\pi/2$, as for the strip. Note that f reaches infinity for $\theta = 0$ with bodies having almost the same horizontal and vertical extents for which higher-order Taylor expansion is necessary. For $d^2 = h^2 - l^2 \ll (h^4 + l^4)/(z_0 + a)^2$ this implies the fourth power of h and l :

$$\mathcal{W}_{\psi_{\tilde{c}}|} \delta T(, z=0)(x_0, a) \simeq 4 \left(\frac{\sin I'}{\sin I'} \right)^2 alhc^{i(-2I'+3\frac{\pi}{2})} \left[\frac{1}{(z_0+a)^3} + 3 \frac{(h/2)^4 + (l/2)^4}{(z_0+a)^7} \right]. \tag{37}$$

3.7. Summary and Discussion

Analysis of magnetic potential fields anomalies using the continuous wavelet transform can be done without the need to reduce the data to the pole or to the equator. As shown by the above results summarized below, the interpretation is made via wavelet coefficients of the anomaly field itself.

Geometrical analysis of modulus maximum lines of either the real or imaginary parts of complex wavelet

coefficients gives a convergence point at the location of a local source (horizontal line). When sources are extended (step, strip, and prism) and have uniform magnetization, there is convergence at the center of the object for modulus maxima lines at large dilations while the convergence is near the upper borders of the object at smaller dilations (when the source is not too deep). For extended sources this also depends on the choice of the derivative order [Moreau *et al.*, 1999].

The modulus maximum line of complex wavelet coefficients is a vertical through the location of a local source (such as a horizontal line), and the modulus along this maximum line allows one to find the depth and homogeneity degree by linear regression of bilogarithmic plots (classical least squares can be used). When sources are extended (step, strip, and prism) and have uniform magnetization, the modulus maxima at large dilations form a vertical line pointing to the center of the source; at small dilations the modulus maxima do not form vertical lines, except for a vertical step or strip (and possibly at vertical borders of a prism) but rather curves pointing near to the upper borders of the object with an angle linked to the dip angle.

For these extended sources with finite height h a

generic law extracted from a multipole expansion gives an estimate of the extent of the source. The first-order expansion is associated with linear fits in the bilogarithmic plot corresponding to an equivalent local source; this depends on three parameters, the depth z_0 , the slope β (linked to the homogeneity degree), and a third term k (linked to the intensity). The second-order term implies a transformation of residuals from the previous linear fits in bilogarithmic plots and provides an alternative means of regression which is deterministic (equation (28)). This gives a function $H(a; z_0, \beta, k)$ which should become a constant for large a for the best a priori model (z_0, β, k) . A correction factor must be applied to obtain the height of the source (equations (32) and (36) and Figure 10). This can also be used as a measure of the uncertainty in the estimated location of sources.

The phase along modulus maxima lines at large dilations tends to a limiting value which is not dependent on a possible dip angle of these extended sources with finite height:

$$\Phi_{\psi_c^\gamma|\delta T} = -2I' + k_\beta \frac{\pi}{2} \pmod{2\pi}, \quad (38)$$

where k_β corresponds to the nature of the source and the order γ of the wavelet; $k_\beta = \gamma + 2$ for a line, a strip or a prism, and $k_\beta = \gamma + 1$ for a right step (and $k_\beta = \gamma - 1$ for a left step). More precisely, k_β is linked to the homogeneity degree. In some cases this is equal to $-\beta = \gamma - \alpha$, and this corresponds to a multipole magnetization whose sum of angles of successive derivatives is a multiple of 2π (or $\Theta_n = 0 \pmod{2\pi}$ in equation (15)).

For other extended sources having a very large extent ($h \rightarrow \infty$), Taylor expanding for $z_0 + a \gg h$ is not possible. It is nevertheless possible to expand wavelet coefficients for $z_1 + a \gg z_1$; this shows that the “depth” as previously estimated is the top depth z_1 instead of the average z_0 , and both the homogeneity degree and limit phase do not obey the above laws. Let us consider the infinite strip which is a typical model used in the classical analytic signal method. The expression for its wavelet coefficients is given by (29) whose first term (with $z_2 \rightarrow \infty$) equals 0; it is governed by the second-order term (with z_1) for any dilation a . This implies that the homogeneity degree α is increased by 1 (-1 instead of -2 for a finite strip), and the phase is decreased by the dip angle ($-2I' + \theta + \pi$ instead of $-2I' + 3\pi/2$).

We have shown analytical results for the total magnetic field anomaly, as due to a 2-D body of homogeneous magnetization with normal apparent inclination I' . These can also be used on other kinds of potential field data. To put them into analytical results that would be obtained for a magnetic potential anomaly δU , a vertical gravity field anomaly δg_z , or a gravity potential anomaly δV , one can use duality equations between wavelet coefficients as shown in Appendix A:

$$\mathcal{W}_{\psi_c^{\gamma+2}|\delta V(\cdot, z)}(x, a) = a^2 \frac{\mathcal{W}_{\psi_c^\gamma|\delta T(\cdot, z)}(x, a)}{\left(\frac{\sin I'}{\sin I}\right)^2 e^{i(-2I'+\pi)}}, \quad (39)$$

so that $(\gamma + 2)$ -order wavelet coefficients of δV have the same properties as γ -order wavelet coefficients of δT for inclination $I' = \pi/2$. Similarly,

$$\mathcal{W}_{\psi_c^{\gamma+1}|\delta g_z(\cdot, z)}(x, a) = a \frac{\mathcal{W}_{\psi_c^\gamma|\delta T(\cdot, z)}(x, a)}{\left(\frac{\sin I'}{\sin I}\right)^2 e^{i(-2I'+3\frac{\pi}{2})}}, \quad (40)$$

so that $(\gamma + 1)$ -order wavelet coefficients of δg_z have the same properties as γ -order wavelet coefficients of δT for inclination $I' = -\pi/4$. Also

$$\mathcal{W}_{\psi_c^\gamma|\delta U(\cdot, z)}(x, a) = \frac{\mathcal{W}_{\psi_c^\gamma|\delta U(\cdot, z)}(x, a)}{\frac{\sin I'}{\sin I'} e^{i(-I'+\frac{\pi}{2})}}, \quad (41)$$

so that γ -order wavelet coefficients of δg_z have the same properties as γ -order wavelet coefficients of δU for inclination $I' = \pi/2$.

4. Aeromagnetic Data

4.1. Survey of French Guiana and Geological Setting

The region of interest for the application of the wavelet transform technique is located between Cayenne and Kourou, in French Guiana (Figure 11). To introduce the geological setting, let us first recall that this forms part of the Guiana Shield, which is made up of an Archean complex and a widely developed Paleoproterozoic succession including metamorphosed sedimentary and volcanic formations and granitic and medium- to high-grade metamorphic terrains and Mezoproterozoic formations at its northern and southern edges [Milési *et al.*, 1995; Vanderhaeghe *et al.*, 1998]. The opening of the North Guiana Trough began with the formation, in a sinistral strike-slip setting, of pull-apart basins in which the Upper Detrital Formation was deposited (after 2120 Ma). Associated with more recent activity due to the extensive tectonics of the early opening of the Atlantic Ocean (200 Ma), Permo-Triassic magmatism has emplaced clusters of dolerite dikes striking NNW and NNE [Deckart, 1995; Deckart *et al.*, 1997]. This geological setting is similar to that found in West Africa, with large ore deposits. As Guiana has been greatly underexplored in comparison, recent exploration interest led to a new survey.

An airborne survey including radiometric and aeromagnetic data (total field intensity) has been carried out by CGG-Géotrex (Compagnie Générale de Géophysique) for BRGM (Bureau des Recherches Géologiques et Minières) in 1996 [Delor *et al.*, 1997]. A total distance of 135,000 km has been flown at a low speed (~ 250 km/h) and a low flight level (~ 120 m clearance). The interline distance was 0.25, 0.5, or 1 km (500 m in the area of interest to us). Using differential GPS, the resolution of data after processing is better than 10 m; sampling interval is ~ 7 m along profiles (constant time sampling interval of 0.1 s). In French Guiana the main magnetic field had inclination $I = 21^\circ$ and declination

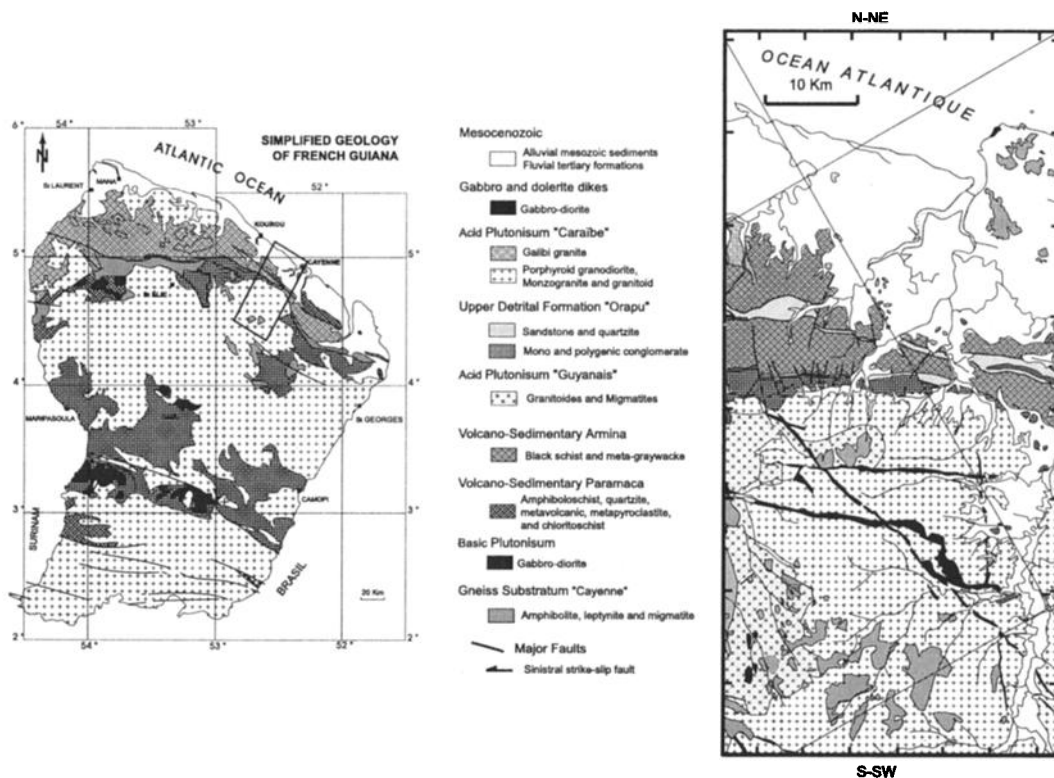


Figure 11. Simplified geological map. (The boxed area between Cayenne and Kourou defines the area of interest to us, shown in more detail on the right side.)

$D = -16.5^\circ$, and the lines were flown in a $N30^\circ E$ direction which means an apparent inclination of $\sim 30^\circ$ when striking anomaly structures of induced magnetization perpendicularly. The reference station for diurnal corrections was located in the Cayenne area. The confidence in the final magnetic data is better than ± 3.8 nT (standard deviation of misfit between crosslines and lines over the whole survey before leveling).

4.2. Profiles and Anomalies of Interest

A set of 27 profiles each of 80 km length has been transformed using wavelets (see central profile in Figure 12). We have analyzed the extrema lines for three singular features: two dikes from the Permo-Triassic and a sinistral strike-slip fault of the Upper Detrital Formation. The geology is revealed magnetically because of the high magnetization of gabbro and diorite of dikes contrasting with the low magnetization of "Caraïbe" and "Guyanais" acid plutonic rocks. The origin of the magnetic anomaly of the fault is in the high magnetization of the Paramaca volcano-sedimentary series (Figure 11).

4.3. Depth: From the Real Part

We first computed the real wavelet coefficients of each profiles (using ψ_x^2). Figure 12 shows typical features of the region, obtained on the central profile. Above the dikes and the fault sources, the wavelet coefficients plotted as a function of altitude exhibit tracks forming

cone-like structures. In wavelet theory these are typical cones for local singularities located at their top: The dikes and the fault are local singularities characterized in the wavelet domain by these cone-like structures.

Interpretation by geometrical continuation of the extrema lines down to their intersections allows one to model the sources. Figure 13 shows the depth of homogeneous sources that have been estimated by picking the two dikes and the fault on all profiles; these values have been corrected for flight altitude and are almost all positive (a very few have very small values of < 50 m corresponding to hills having strongly variable ground level). The fault (right side on Figure 13) has a deeper magnetic response (200 m down to 1 km) than the two dikes (< 400 m); in the central profile, one gets the following depths z_0 (from the SSW to the NNE): 370 m (SSW dike), 250 m (middle dike), and 930 m (the fault). Note that horizontal positions follow what would have been obtained by classical methods based on the locations of the extrema of the analytic signal or the gradient of the field reduced to the pole. This method gives realistic depth estimates with regard to the geological nature of the sources. Other computations using the Euler deconvolution method (not shown) have given lower depth estimates, with negative values when corrected for flight altitude [Sailhac *et al.*, 1997]. This traduces the problem of noise effect in Euler deconvolution which is automatically solved by upward continuation in the wavelet method.

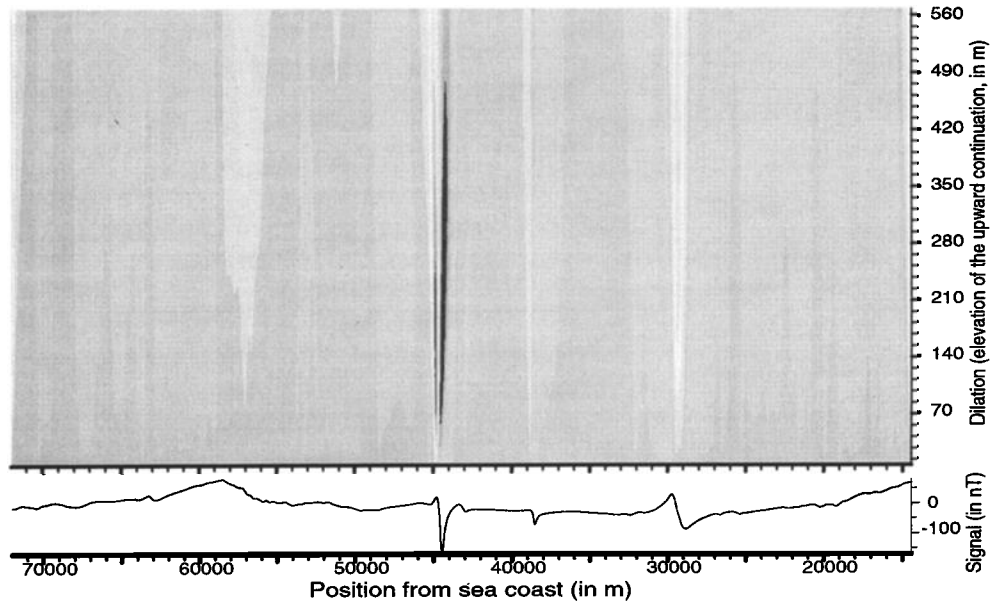


Figure 12. Typical SSW-NNE profile of the survey: Total magnetic field anomaly and its wavelet transform coefficients (maxima are in dark and minima in clear shading).

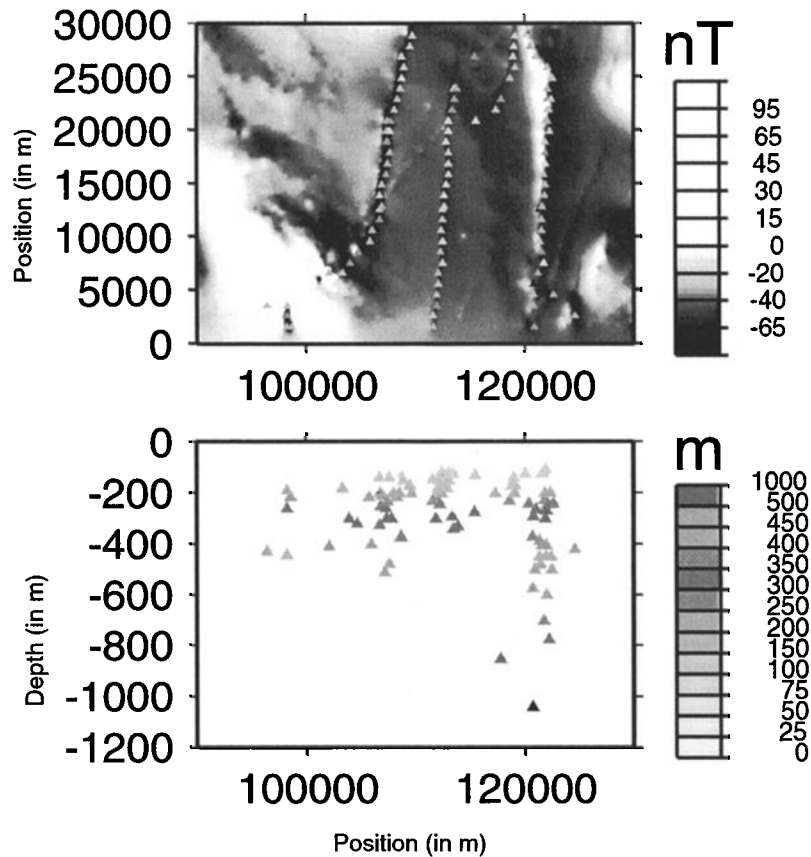


Figure 13. Imaging sources from the use of 1-D real wavelets: Each profile anomaly provides one source location. For the set of profiles in the area this maps horizontal positions and depths (top) as seen from above superimposed on the anomalies in grey scale and (bottom) its vertical cross section projection. For the central profile one gets the following depths z_0 (from the SSW to the NNE): 370 m (SSW dike), 250 m (middle dike), and 930 m (the fault).

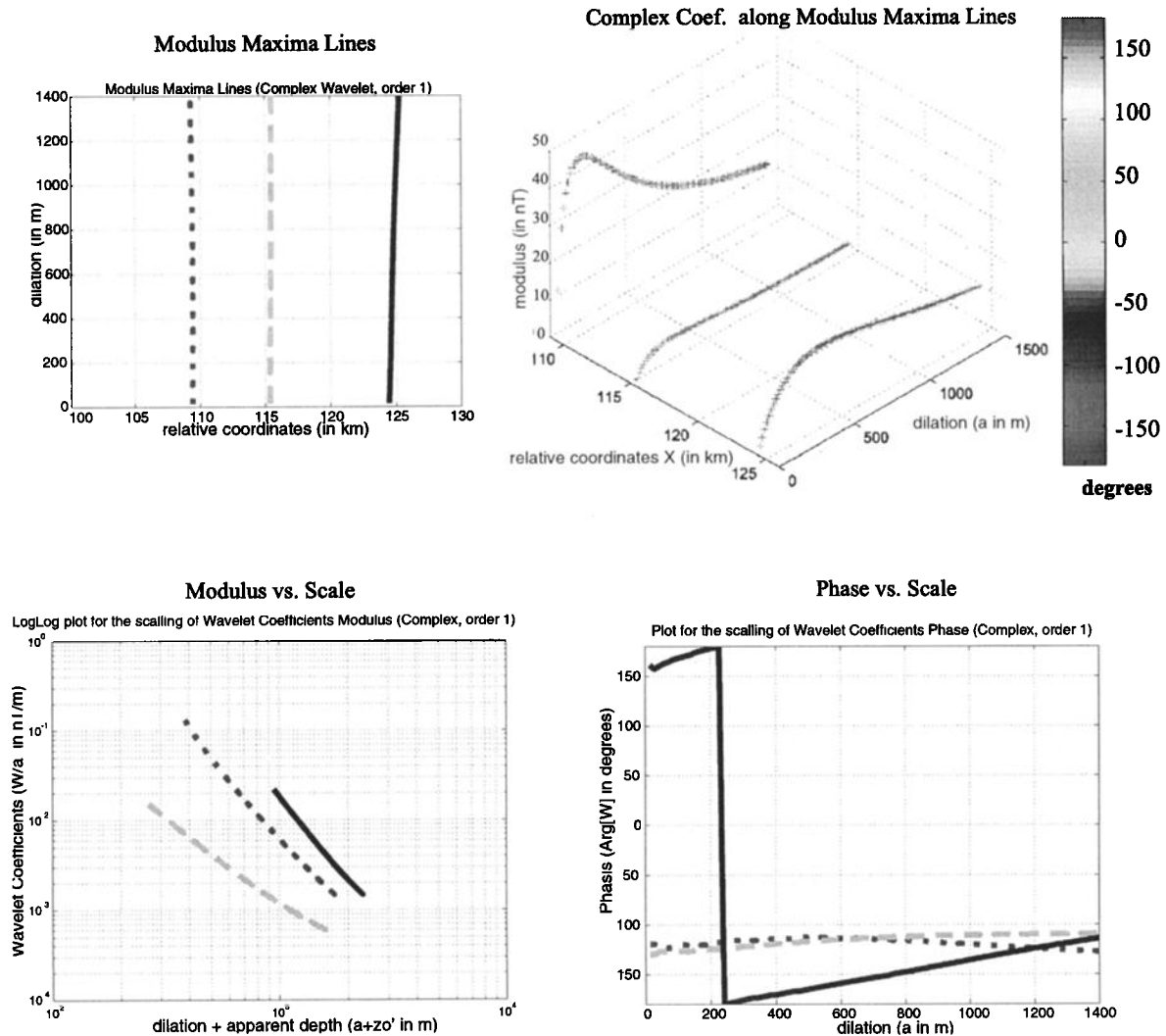


Figure 14. Characterization of the sources from the use of 1-D complex wavelets: (top) The modulus maxima lines and the phase along these lines obey (bottom) scaling relations characterizing the two dikes (dotted and dashed) and the fault (plain); (bottom left) homogeneity degree is given by the plot of $\log(|W_a|/a)$ versus $\log(a + z_0)$, and (bottom right) inclination is given by the limit of $\text{Arg}(W_a)$ for large a .

4.4. Homogeneity Degree: From the Modulus

Using depth estimated from the geometrical procedure on modulus maxima lines of the real wavelet coefficients (section 4.3), we have estimated the homogeneity degrees from the modulus maxima lines of the complex coefficients calculated on the central profile of Figure 12.

As shown on Figure 14, modulus maxima lines are both vertical for the two dikes and display an angle $\theta \simeq 50^\circ$ for the fault, this gives a rough estimate of its angle (dipping NNE). Using the depths z_0 estimated from real wavelets, the linear regression of $\log(|W_c^1(a)|/a)$ versus $\log(a + z_0)$ implies a homogeneity degree of $\alpha = -1.9$ (the slope is $\beta = -2.9$ and the structural index is $N = 0.9$) for the SSW dike and the fault and of $\alpha = -0.9$ (the slope is $\beta = -1.9$ and the struc-

tural index is $N = -0.1$) for the middle dike. The SSW dike and the fault have an homogeneity degree which is in the range of that of a prism or a strip [Moreau, 1995], near to that of a horizontal pipe ($\alpha = -2.0$). This corresponds with magnetization anomalies as expected (section 4.2): a gabbro-dioritic dike of high magnetization and a fault whose magnetic signature is the Paramaca volcano-sedimentary series. “fault”: this can also be the signature of an edge of a sill-like source created by the Paramaca volcano-sedimentary abutting against the coastal sedimentary rocks.

The middle dike is seen with a surprising homogeneity degree which is near to that of a step ($\alpha = -1.0$) rather than a prism. A first interpretation of this value is that there is also, associated with this dike, a contrast in the magnetization of the background. Indeed, a contact with the Cayenne Series (composed of amphi-

bolites, leptynites and migmatites) has been recognized (see Figure 11); they constitute a surface of migrated ferromagnetic elements. This remark agrees with the shape of the observed anomaly (see Figure 12) as compared to the synthetic one (appearing on Figure 7). A second interpretation is that this is a strip-like source as expected but with an infinite height extent (such that the first term in equation (34) tends to zero and the second term implies the observed exponent $\beta = -2$). In this case, the significance of estimated depths is not the middle of the object but for the top of the dike (as in the classical analytic signal interpretation method).

4.5. Inclination: From the Phase

The plots of the phase of the complex coefficients versus scale exhibit a different behavior for the dikes and the "fault" (see Figure 14). A constant phase of $\sim -120^\circ$ is observed for the two vertical dikes. A moving value from 150° to -120° is observed for the inclined "fault". These differences are due to the dependence of the phase on the dip angle of the source that is significant for small scales and disappears for large scales when the source has a finite extent. In this case, the limit for large scales can be used to obtain the inclination (equation (43)).

The value of -120° gives an apparent inclination of about 15° (modulo 180°) for the vertical dike and the fault whose homogeneity degree is $\alpha = -2.0$. This implies that values of inclination I and declination D of the source are similar to the inclination I_n and declination D_n of the normal field (for which $I' = 30^\circ$ in the case that the profile is perpendicular to the source).

For the vertical dike whose homogeneity degree is $\alpha = -1.0$, one obtains the same value for the apparent inclination by assuming this is a dike of infinite extent while one obtains a value of $\sim -30^\circ$ (modulo 180°) for a finite step. However it is unlikely that the Cayenne Series has a reversed remanent magnetization. Therefore this vertical dike is probably of large extent with a top at ~ 250 m depth and a magnetization with apparent inclination of $\sim 15^\circ$ (modulo 180°).

5. Conclusion and Perspectives

The wavelet technique is aimed at analyzing both the geometry and locations of the sources of potential fields via relations of derivatives of the upward continued field. This can be applied to any potential fields and components. A geometrical interpretation of the scaling over the cone-like structure of the real wavelet coefficients induced by the source can be used for modeling. An automatic depth to source determination is based upon adjustments of a scaling law for the modulus of complex wavelet coefficients (of $|\mathcal{W}_a|/a^\gamma$ versus $a + z_0$). This can be applied for some nonlocal sources such as prismatic bodies where residuals of a simple power scaling law form an estimate of the extent of the source; this has been recently successfully applied

to the interpretation of a gravity profile crossing the Himalayas [Martelet *et al.*, 2000].

The application to high-resolution aeromagnetic profiles of French Guiana has shown the utility of the technique for the interpretation of magnetic structures. There is no need to reduce to the pole, and the phase of complex wavelet coefficients indicates the inclination of the magnetization. This is helpful, especially in areas where geophysical prospecting is the only access to information on depths of structures, as we have shown for dikes and a fault in Guiana.

Further possibilities with other wavelets of this kind could be explored for reduction to the pole in the first instance. This wavelet technique combines different directions of derivative of the field. Also note that this could be used for interpretation of surveys where different components of the field have been simultaneously recorded: The wavelet analysis of the magnetic potential U is equivalent to the analysis of the horizontal and vertical components H and Z that are upward continued to different levels.

This article is the second of a series; forthcoming ones will relate to statistics of the sources, automation of the technique, considerations of large-scale asymptotic behavior, and application of 2-D wavelets to aeromagnetic maps.

Appendix A: Wavelet Coefficients Versus Green Function

Here we show useful relations between wavelet coefficients of a potential field due to a 2-D body of constant source density and the Green's function V (which corresponds to its gravity potential). Factors corresponding to the nature of the field (mass or magnetization intensity) have been omitted for the relations to be general (these are given by Telford *et al.* [1990] or Blakely [1996]). From equations (5), and (7), complex wavelet coefficients of V are given by

$$\mathcal{W}_{\psi_c^\gamma|V(\cdot, z)}(x, a) = a^\gamma \left(\frac{\partial}{\partial x} \right)^{\gamma-1} \left[\frac{\partial V(x, z+a)}{\partial x} + i \frac{\partial V(x, z+a)}{\partial z} \right]. \quad (\text{A1})$$

Now let us introduce a complex gravity field anomaly $\delta g_c = \delta g_x + i\delta g_z$, whose real part is given by the horizontal gravity field anomaly $\delta g_x = \partial V/\partial x$ and whose imaginary part is given by the vertical gravity field anomaly $\delta g_z = \partial V/\partial z$ (where the z axis is downward oriented). With this definition, δg_c is actually a complex function of the complex variable $\zeta = x + ia$, which is defined from δg_x with the Hilbert transform: $\delta g_c = (1 + i\mathcal{H})\delta g_x$. Hence complex wavelet coefficients of V are

$$\mathcal{W}_{\psi_c^\gamma|V(\cdot, z)}(x, a) = a^\gamma \left(\frac{\partial}{\partial x} \right)^{\gamma-1} \delta g_c(x, z+a). \quad (\text{A2})$$

Similarly, the complex wavelet coefficients of δg_z are

$$\mathcal{W}_{\psi_c^\gamma|\delta g_z(\cdot, z)}(x, a) = a^\gamma e^{-i\frac{\pi}{2}} \left(\frac{\partial}{\partial x} \right)^\gamma \delta g_c(x, z + a). \quad (\text{A3})$$

Then we consider the magnetic potential anomaly produced by a set of elementary magnetization vectors with declination D and inclination I within a normal field of declination D_n and inclination I_n . Along profiles perpendicular to the sources and making an angle φ with geographic north (Figure 4), a simplification follows by introducing an apparent inclination I' corresponding to a geomagnetic south-north profile [de Gery and Naudy, 1957]. Thus the magnetic potential anomaly δU is given by an oblique derivative of V in direction I' :

$$\mathcal{W}_{\psi_c^\gamma|\delta U(\cdot, z)}(x, a) = a^\gamma \frac{\sin I}{\sin I'} e^{-iI'} \left(\frac{\partial}{\partial x} \right)^\gamma \delta g_c(x, z + a). \quad (\text{A4})$$

Eventually, we consider the magnetic total field anomaly. Similar to the apparent inclination (magnetization direction), one can introduce an apparent normal inclination I'_n (normal field direction). Thus the total magnetic field anomaly δT at (x, z) is given by two conjugated symmetrical and antisymmetrical functions δT_1 and δT_2 . Let us introduce the mean apparent inclination $\mathfrak{S} = (I' + I'_n)/2$ (such that in the special case of normal apparent inclination, one gets $\mathfrak{S} = I' = I'_n$); this now reads

$$\delta T = \frac{\sin I}{\sin I'} \frac{\sin I_n}{\sin I'_n} [-\delta T_1 \cos 2\mathfrak{S} + \delta T_2 \sin 2\mathfrak{S}], \quad (\text{A5})$$

where δT_1 and δT_2 are defined by second-order derivatives of the Green's function V :

$$\begin{aligned} \delta T_1(x, z) &= \frac{\partial^2}{\partial x^2} V(x, z) = -\frac{\partial^2}{\partial z^2} V(x, z), \\ \delta T_2(x, z) &= -\frac{\partial^2}{\partial x \partial z} V(x, z). \end{aligned} \quad (\text{A6})$$

Complex wavelet coefficients of δT are

$$\begin{aligned} \mathcal{W}_{\psi_c^\gamma|\delta T(\cdot, z)}(x, a) &= \\ -a^\gamma \frac{\sin I}{\sin I'} \frac{\sin I_n}{\sin I'_n} e^{-i2\mathfrak{S}} \left(\frac{\partial}{\partial x} \right)^{\gamma+1} \delta g_c(x, z + a). \end{aligned} \quad (\text{A7})$$

Appendix B: Modulus Maxima Lines of Real Wavelet Coefficients

We look for the geometry of modulus maxima lines from real wavelet coefficients and its relation to the mean apparent inclination \mathfrak{S} (equation (A5)). Let us consider the following characteristic ratio function:

$$R^\gamma(x, a) = \frac{\partial^{\gamma+1} \delta T_1(x, -a)}{\partial x^{\gamma+1}} / \frac{\partial^{\gamma+1} \delta T_2(x, -a)}{\partial x^{\gamma+1}}. \quad (\text{B1})$$

Now, if we look for the modulus maxima of $\mathcal{W}_{\psi^\gamma|\delta T(\cdot, z)}$ (maxima of a profile while dilation is kept constant), the question is reduced to searching for the zero-set

of $\mathcal{W}_{\psi^{\gamma+1}|\delta T(\cdot, z)}$. Algebraic manipulations lead to the equation $R^\gamma(x, a) = \tan(2\mathfrak{S})$ (respectively $R^\gamma(x, a) = -\cot(2\mathfrak{S})$) for the definition of the modulus maxima lines (x, a) of $\mathcal{W}_{\psi_c^\gamma|\delta T(\cdot, z)}$ (respectively $\mathcal{W}_{\psi_c^{\gamma+1}|\delta T(\cdot, z)}$).

Thus their geometry is controlled by the derivative order γ and the mean apparent inclination $\mathfrak{S} = (I' + I'_n)/2$. Nevertheless, when considering the modulus of the complex wavelets coefficients, it is obvious (from equation (A7)) that the derivative order γ , but not \mathfrak{S} , controls the geometry of modulus maxima lines.

Appendix C: Complex Variables Method and Numerical Applications

A general formulation for the direct calculation of the complex wavelet coefficient due to a 2-D body of any shape can be obtained with the help of complex variables $w = X + iZ$, where $X = x - x_0$ and $Z = z_0 + a$ are the horizontal and vertical coordinates, respectively, from the source at coordinates x_0 and z_0 (as used in section 3). This method has been previously applied to the calculation of derivatives of any order from the vertical gravity component [Kwok, 1989].

This allows us to write the coefficients at (x, a) of the complex wavelets ψ_c^1 for the total magnetic field anomaly due to the 2-D body of contour $(x_0, z_0) \in S$:

$$\begin{aligned} \mathcal{W}_{\psi_c^1|\delta T(\cdot, z=0)}(x, a) &= \\ 4 \left(\frac{\sin I}{\sin I'} \right)^2 a e^{i2I'} \iint_S \frac{dx_0 dz_0}{((x-x_0)+i(z_0+a))^{\mathfrak{S}}}. \end{aligned} \quad (\text{C1})$$

For ψ_c^γ and any derivative order $\gamma \in \mathbb{R}_*^+$ this becomes

$$\begin{aligned} \mathcal{W}_{\psi_c^\gamma|\delta T(\cdot, z=0)}(x, a) &= \\ 2\Gamma(\gamma + 2) \left(\frac{\sin I}{\sin I'} \right)^2 a^\gamma e^{i2I'} \iint_S \frac{dx_0 dz_0}{((x-x_0)+i(z_0+a))^{\gamma+2}}. \end{aligned} \quad (\text{C2})$$

As shown by Kwok [1989], because the integrand is analytic, the double integral above can be simplified using the complex variable $w = (x - x_0) + i(z_0 + a)$. The complex form of Green's theorem gives integrations over the closed contour C in the complex plane $(x_0, -iz_0)$:

$$\begin{aligned} 2 \operatorname{Re} \iint_S \frac{dx_0 dz_0}{((x-x_0)+i(z_0+a))^{\gamma+2}} &= \operatorname{Im} \oint_C \frac{\bar{w} dw}{w^{\gamma+2}}, \\ 2 \operatorname{Im} \iint_S \frac{dx_0 dz_0}{((x-x_0)+i(z_0+a))^{\gamma+2}} &= -\operatorname{Re} \oint_C \frac{\bar{w} dw}{w^{\gamma+2}}. \end{aligned} \quad (\text{C3})$$

Hence, equation (C2) reads

$$\begin{aligned} \mathcal{W}_{\psi_c^\gamma|\delta T(\cdot, z=0)}(x, a) &= \\ \Gamma(\gamma + 2) \left(\frac{\sin I}{\sin I'} \right)^2 a^\gamma e^{i(-2I'+3\frac{\pi}{2})} \oint_C \frac{\bar{w} dw}{w^{\gamma+2}}. \end{aligned} \quad (\text{C4})$$

Also, the real and imaginary parts give the real wavelet coefficients, $\mathcal{W}_{\psi_x^\gamma}(x, a)$ and $-\mathcal{W}_{\psi_z^\gamma}(x, a)$, respectively.

For numerical applications on closed n -sided polygonal 2-D bodies, one may consider the case of integer

derivative order $\gamma \in \mathbb{N}^*$. To the coordinates (x_j, z_j) of each vertex $j \in \{1, \dots, n\}$, one associates the series of complex numbers $w_j = (x - x_j) + i(z_j + a)$ (and $w_{n+1} = w_1$). This is used to transform equation (C4) into

$$\mathcal{W}_{\psi_{\gamma}|\delta T(\cdot, z=0)}(x, a) = \frac{-(\gamma+1)a^\gamma}{(\gamma-1)(\gamma-2)} \left(\frac{\text{Sin}I}{\text{Sin}I'}\right)^2 e^{i(-2I'+3\frac{\pi}{2})} \sum_{j=1}^n e^{-2i\Phi(w_{j+1}-w_j)} \left[\frac{e^{-i(\gamma-2)\Phi(w_{j+1})}}{|w_{j+1}|^{\gamma-2}} - \frac{e^{-i(\gamma-2)\Phi(w_j)}}{|w_j|^{\gamma-2}} \right], \quad (\text{C5})$$

where $\Phi(w) = \text{Arg}(w)$ is the argument of w .

Notation

$f(x)$	function of a real variable x .
$\hat{f}(u)$	Fourier transform of $f(x)$, equal to $\int_{-\infty}^{+\infty} dx f(x) e^{-i2\pi ux}$.
\mathcal{H}	Hilbert transform ($\mathcal{H}[f](x) = \int_{-\infty}^{+\infty} dx' \frac{f(x')}{\pi(x-x')}$).
\mathcal{D}_a	dilation operator ($\mathcal{D}_a f(x) = (1/a)f(x/a)$).
$P(x)$	Poisson kernel (upward continuation filter, at level +1), equal to $P_1(x)$.
$P_a(x)$	dilated Poisson kernel (upward continuation filter, at level +a), equal to $\mathcal{D}_a P(x)$.
i	square root of -1.
$\partial_x = \frac{\partial}{\partial x}$	partial differential operator with respect to x .
$\psi_x^\gamma(x)$	real wavelet (of order γ) whose first derivative is in x .
$\psi_z^\gamma(x)$	real wavelet (of order γ) whose first derivative is in z .
$\psi_c^\gamma(x)$	complex wavelet (of order γ).
$\psi_a^\gamma(x)$	wavelet (of order γ) dilated by dilation a .
$\mathcal{W}_{\psi\gamma \phi_0}(x, a)$	wavelet coefficient of ϕ_0 (by convolution of $\phi_0(x)$ with $\psi_a^\gamma(x)$, for $x \in \mathbb{R}$).
$\mathcal{W}_{\psi\gamma \phi(\cdot, z)}(x, a)$	wavelet coefficient of $\phi(\cdot, z)$ (by convolution of $\phi(x, z)$ with $\psi_a^\gamma(x)$, for $x \in \mathbb{R}$).
$\Phi_{\psi\gamma \phi(\cdot, z)}(x, a)$	argument (or phase) of the wavelet coefficient $\mathcal{W}_{\psi\gamma \phi(\cdot, z)}(x, a)$.
$\Gamma(x)$	Gamma function of the real variable x (for $n \in \mathbb{N}$, $\Gamma(n+1) = n!$).
\bar{w}	conjugate of the complex variable w .
I, D	inclination and declination of the magnetization vector.
I_n, D_n	inclination and declination of the normal field.
I'	apparent inclination of the magnetization vector.
I'_n	apparent inclination of the normal field.
\mathfrak{S}	mean apparent inclination, equal to $(I' + I'_n)/2$.

Acknowledgments. This paper benefited from comments made by Associate Editor Kathy Whaler and two reviewers Alan Reid and Dhananjay Ravat. We also had numerous discussions with our colleagues Matthias Holschneider, Guillaume Martelet, and Ginette Saracco. This is IGP contribution number NS 1680.

References

- Baranov, W., *Potential Fields and Their Transformations in Applied Geophysics, Geoexplor. Monogr. Ser.*, vol. 6, 121 pp., Gebruder Borntraeger, Stuttgart, Germany, 1975.
- Barbosa, V.C.F., J.B.C. Silva, and W.E. Medeiros, Stability analysis and improvement of structural index estimation in Euler deconvolution, *Geophysics*, **64**, 48-60, 1999.
- Bhattacharyya, B.K., Design of spatial filters and their application to high-resolution aeromagnetic data, *Geophysics*, **37**, 68-91, 1972.
- Biegert, E.K., and P.S. Millegan, Beyond recon: The new world of gravity and magnetics, *Leading Edge*, **17**, 41-42, 1998.
- Blakely, R.J., *Potential Theory in Gravity and Magnetic Applications*, 441 pp., Cambridge Univ. Press., New York, 1996.
- Deckart, K., Etude du magmatisme associé au rifting de l'Atlantique Central et Sud: Géochronologie $^{40}\text{Ar}/^{39}\text{Ar}$ et géochimie des intrusions Jurassiques de Guinée et de Guyane française, Surinam, et Crétacé au Brésil, thèse de doctorat, 250 pp., Univ. de Nice, Nice, France, 1995.
- Deckart, K., G. Féraud, and H. Bertrand, Age of Jurassic continental tholeiites of French Guiana, Surinam and Guinea: Implications for the initial opening of the central Atlantic Ocean, *Earth Planet. Sci. Lett.*, **150**, 205-220, 1997.
- de Gery, J. C., and H. Naudy, Sur l'interprétation des anomalies gravimétriques et magnétiques, *Geophys. Prospect.*, **5**, 421-448, 1957.
- Delor, C., J. Perrin, and C. Truffert, Campagne de géophysique aéroportée en Guyane française. Magnétisme et radiométrie spectrale, *Rap. 39625*, 102 pp., Bur. de Rech. Géol. Min., Orléans, France, 1997.
- Fedi, M., and T. Quarta, Wavelet analysis for the regional-residual and local separation of potential field anomalies, *Geophys. Prospect.*, **46**, 507-525, 1998.
- Galdeano, A., *Traitement des données aéromagnétiques: Méthodes et applications*, thèse de doctorat, 153 pp., Univ. de Paris VI, Paris, 1974.
- Gibert, D., and A. Galdeano, A computer program to perform the upward continuation of potential field data, *Comput. Geosci.*, **11**, 533-588, 1985.
- Grauch, V.J.S., and P.S. Millegan, Mapping intrabasinal faults from high-resolution aeromagnetic data, *Leading Edge*, **17**, 53-55, 1998.
- Gunn, P.J. (Ed), *Airborne magnetic and radiometric surveys*, *J. Aust. Geol. Geophys.*, **17**, 216 pp., 1997.
- Holschneider, M., *Wavelets: An Analysis Tool*, 423 pp., Clarendon, Oxford, England, 1995.
- Hornby, P., F. Boschetti, and F.G. Horowitz, Analysis of potential field data in the wavelet domain, *Geophys. J. Int.*, **137**, 175-196, 1999.
- Hsu, S.-K., D. Coppens, and C.-T. Shyu, Depth to magnetic source using the generalized analytic signal, *Geophysics*, **63**, 1947-1957, 1998.
- Huang, D., Enhancement of automatic interpretation techniques for recognising potential field sources, Ph.D. thesis, 216 pp., Univ. of Leeds, Leeds, England, 1996.
- Kwok, Y.-K., Conjugate complex variables method for the computation of gravity anomalies, *Geophysics*, **54**, 1629-1637, 1989.

- Le Mouél, J.-L., Le levé aéromagnétique de la France: Calcul des composantes du champ à partir des mesures de l'intensité, *Ann. Géophys.*, **26**, 229-258, 1970.
- Martelet, G., P. Sailhac, F. Moreau, and M. Diament, Characterization of geological boundaries using 1-D wavelet transform on gravity data: Theory and application to the Himalayas, *Geophysics*, in press, 2000.
- Milési, J.P., E. Egal, P. Ledru, Y. Vernhet, D. Thiéblemont, A. Cocherie, M. Tegye, B. Martel-Jantin, and P. Lagny, Northern French Guiana ore deposits in their geological setting, in French with English extended abstract, *Chron. Rech. Min.*, **518**, 5-58, 1995.
- Moreau, F., Méthodes de traitement de données géophysiques par transformée en ondelettes. thèse de doctorat, 177 pp., Univ. de Rennes I, Rennes, France, 1995.
- Moreau, F., D. Gibert, M. Holschneider, and G. Saracco, Wavelet analysis of potential fields, *Inverse Probl.*, **13**, 165-178, 1997.
- Moreau, F., D. Gibert, M. Holschneider, and G. Saracco, Identification of sources of potential fields with the continuous wavelet transform: Basic theory, *J. Geophys. Res.*, **104**, 5003-5013, 1999.
- Nabighian, M.N., The analytic signal of two-dimensional magnetic bodies with polygonal cross-section: Its properties and use for automated interpretation, *Geophysics*, **37**, 507-517, 1972.
- Nabighian, M.N., Additional comments on the analytic signal of two dimensional magnetic bodies with polygonal cross-section, *Geophysics*, **39**, 85-92, 1974.
- Paul, M.K., S. Datta, and B. Banerjee, Direct interpretation of two-dimensional structural faults from gravity data, *Geophysics*, **31**, 940-948, 1966.
- Pedersen, L.B., and T.M. Rasmussen, The gradient tensor of potential fields anomalies: Some implications on data collection and data processing of maps, *Geophysics*, **55**, 1558-1566, 1990.
- Pilkington, M., 3-D magnetic imaging using conjugate gradients, *Geophysics*, **62**, 1132-1142, 1997.
- Ravat, D., and P.T. Taylor, Determination of depths to centroids of three-dimensional sources of potential-field anomalies with examples from environmental and geological applications, *J. Appl. Geophys.*, **39**, 191-208, 1998.
- Reid, A.B., J.M. Allsop, H. Grasner, A.J. Millet, and I.W. Somerton Magnetic interpretation in three dimensions using Euler deconvolution, *Geophysics*, **55**, 80-91, 1990.
- Ridsdill-Smith, T.A., and M.C. Dentith, The wavelet transform in aeromagnetic processing, *Geophysics*, **64**, 1003-1013, 1999.
- Sailhac, P., A. Galdeano, D. Gibert, and F. Moreau, Wavelet Based Method for the Interpretation of Aeromagnetic Survey in French Guyana, *Eos Trans. AGU*, **78(46)**, Fall Meet. Suppl., F35, 1997.
- Smith, R.S., J. B. Thurston, T.-F. Dai, and I.N. MacLeod, iSPI-The improved source parameter imaging method, *Geophys. Prospect.*, **46**, 141-151, 1998.
- Telford, W.M., L.P. Geldart, and R.E. Sheriff, Magnetic methods, in *Applied Geophysics*, pp. 62-135, Cambridge Univ. Press, New York, 1990.
- Thompson, D.T., EULDPH: A new technique for making computer-assisted depth estimates from magnetic data, *Geophysics*, **47**, 31-37, 1982.
- Vanderhaeghe, O., P. Ledru, D. Thiéblemont, E. Egal, A. Cocherie, M. Tegye, and J.-P. Milési, Contrasting mechanism of crustal growth. Geodynamic evolution of Paleoproterozoic granite-greenstone belts of French Guiana, *Precambrian Res.*, **92**, 165-193, 1998.
-
- C. Delor, Bureau des Recherches Géologiques et Minières, La Source, Orléans, France.
- A. Galdeano and P. Sailhac, Laboratoire de Géomagnétisme (UMR 7577 du CNRS), Institut de Physique du Globe de Paris, 4 place Jussieu 75252, Paris, France. (galdeano@ipgp.jussieu.fr; sailhac@ipgp.jussieu.fr)
- D. Gibert and F. Moreau, Géosciences Rennes (UPR 4661 du CNRS), Université de Rennes 1, Bât. 15, Beaulieu, 35042 Rennes Cedex, France. (gibert@univ-rennes1.fr; moreau@univ-rennes1.fr)

(Received March 17, 1999; revised January 3, 2000; accepted March 15, 2000.)